Marine and Petroleum Geology 152 (2023) 106225

Contents lists available at ScienceDirect

Marine and Petroleum Geology

journal homepage: www.elsevier.com/locate/marpetgeo

Differential hydrocarbon generation and evolution of typical terrestrial gas-prone source rocks: An example from the Kuqa foreland basin, NW China

Jianliang Liu [a,b], Xianzhang Yang [c], Keyu Liu [a,b,d,*], Zhenping Xu [c], Kun Jia [a], Lu Zhou [c], Hongxing Wei [c], Liang Zhang [c], Shaojun Wu [c], Xinzhuo Wei [a]

[a] School of Geosciences, China University of Petroleum (East China), Qingdao, 266580, China
[b] Shandong Provincial Key Laboratory of Deep Oil and Gas, Qingdao, China, 266580, China
[c] Research Institute of Exploration & Development, PetroChina Tarim Oilfield Company, Korla, 841000, China
[d] Qingdao National Laboratory for Marine Science and Technology, Qingdao, 266071, China

ARTICLE INFO

Keywords:
Hydrocarbon generation and cracking
Kinetics
Mudstone
Carbonaceous mudstone and coal
Sealed gold tube pyrolysis experiment
Kuqa foreland basin

ABSTRACT

Terrestrial gas-prone source rocks are significant for hydrocarbon gas accumulations especially in central and western basins in China. The Kuqa foreland basin in the northern margin of the Tarim Basin, NW China is rich in natural gas with recent discoveries of several large to giant gas-producing fields (e.g., the Kela-2, Dibei, Dabei-1, and Zhongqiu-1 gas fields, etc.) and a proven 3 P gas reserve of over one trillion cubic meters (TCM). This proliferous petroleum province is powered by an effective and diverse gas-prone source rock series in the basin comprising mudstone, carbonaceous mudstone, and coal seams. To date, little systematic research work has been done on the petroleum generation potential of the source rocks. This has seriously restricted the assessment of petroleum resources and further exploration in the frontier areas of the basin. A sealed gold tube pyrolysis approach was employed to simulate the oil and gas generation and cracking yields for the aforementioned three types of source rock. Compared with typical Type I and II_1 kerogens, the three types of source rocks in the Kuqa foreland basin are characterized by (1) far less hydrocarbon yield (150 mg/g TOC) with comparatively larger amounts of CO_2 (310 mg/g TOC), (2) a limited capacity and narrower window (0.5%–1.08% Ro) for oil generation, and (3) a much earlier secondary cracking for bulk oil to light oil and gases (>0.86% Ro for mudstone and >1.08% Ro for both carbonaceous mudstone and coal). All the source rocks are gas-prone, and significant amount of gas can still be generated during an over-mature stage. The kinetic parameters obtained allow us to model hydrocarbon generation in the Kuqa foreland basin more realistically. It is concluded that (1) two episodes of hydrocarbon generation occurred with hydrocarbon gases being mainly generated during the later stage (12–3 Ma); and (2) the depocenter of the basin is capable of supplying massive high-mature gases as late as in the Quaternary, which is crucial for the formation of giant gas fields. The findings provide new insight on the reconstruction of oil and gas accumulation processes and further hydrocarbon exploration in the basin.

1. Introduction

Terrestrial source rocks can be well developed in different types of lake basins: overfilled, balanced fill, and underfilled lake basins (Bohacs et al., 2000). Thick and widespread lacustrine source rocks with good quality of organic matters and reservoirs assemblages are important for hydrocarbon explorations in many areas including Africa, South America, southeast Asia and China (Katz, 1995; Harouna et al., 2017; Xu et al., 2019a, 2021; Ahmed et al., 2022). Oil-prone terrestrial source rocks typically develop in balance fill and underfilled lake basins (Bohacs et al., 2000), and are primarily be found in basins in eastern China, such as Bohai Bay and Songliao basins (Zhao et al., 2004; Hao et al., 2007; Xu et al., 2019b; Wang et al., 2023). While gas-prone source rocks, including mudstone, carbonaceous mudstone, and coal, generally developed in overfilled lake basin (Bohacs et al., 2000), and are usually be found in central and western basins in China (e.g., Tarim, Junggar, and Tuha basins) (Gao et al., 2009; Liu et al., 2018; Huang et al., 2019; Hu et al., 2020). Many large (condensate) gas fields have been

* Corresponding author. School of Geosciences, China University of Petroleum (East China), Qingdao, 266580, China.
E-mail address: liukeyu@upc.edu.cn (K. Liu).

https://doi.org/10.1016/j.marpetgeo.2023.106225
Received 21 November 2022; Received in revised form 10 March 2023; Accepted 14 March 2023
Available online 16 March 2023

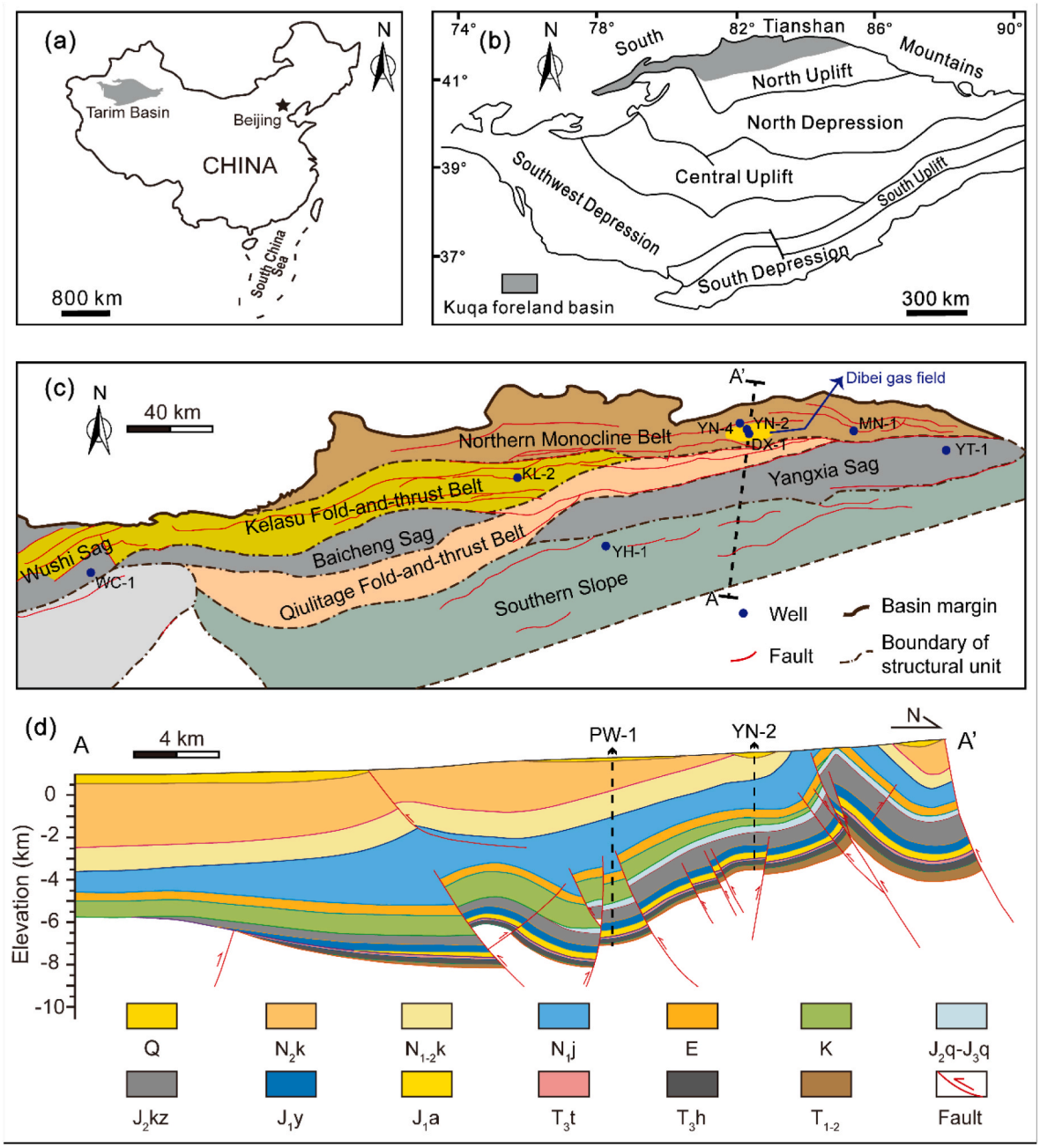

Fig. 1. Location maps of the Tarim Basin (a) and the Kuqa foreland basin (b); (c) Distribution of major structural belts and sags in the Kuqa foreland basin; (d) Near N–S cross section (A-A′) through the Kuqa foreland basin showing structural zones and key stratigraphic intervals. PW-1 in (d) marks the location of a pseudo well modeled. Q = Quaternary; N_2k = Upper Neogene Kuqa Formation; $N_{1\text{-}2}k$ = Lower to Upper Neogene Kangcun Formation; N_1j = Lower Neogene Jidike Formation; E = Paleogene; K = Cretaceous; J_2q-J_3q = Middle Jurassic Qiakemake to Upper Jurassic Qigu formations; J_2kz = Middle Jurassic Kezilenuer Formation; J_1y = Lower Jurassic Yangxia Formation; J_1a = Lower Jurassic Ahe Formation; T_3t = Upper Triassic Taliqike Formation; T_3h = Upper Triassic Huangshanjie Formation; $T_{1\text{-}2}$ = Lower to Middle Triassic.

discovered in these lacustrine basins, especially in the Kuqa foreland basin in northwestern China (Du et al., 2012; Lu et al., 2018; Yang et al., 2022), confirming the significance of gas-prone terrestrial source rocks.

Hydrocarbon generation is controlled by thermal cracking of sedimentary organic matters, which can be described by organic matter maturation kinetic models (Quigley et al., 1987; Tissot et al., 1987). The generative process is generally represented as a series of independent first-order reactions, which are characterized by a particular activation energy and a frequency factor or Arrhenius constant (Mangotra et al., 1995; Peters et al., 2015). Owing to varying source inputs, depositional environments and geological evolution, great differences exist among the generative kinetics in various source rocks or in the same source rock but with different organofacies (Tissot et al., 1987; Ungerer and Pelet, 1987; Burnham and Braun, 1990; Tegelaar and Noble, 1994; Peters et al., 2006, 2015). For example, relatively narrow activation energies are found in lacustrine derived organic matters due to their overall homogeneity, while broad hydrocarbon generation ranges are usually obtained in terrestrial organic matters because it is characterized by various chemical structures and associated chemical bonds in the preserved organic matters (Schenk et al., 1997; Dieckmann, 2005). Peters et al. (2006) also quantified a great level of uncertainty in kinetic responses for kerogen decomposition to petroleum even in source rocks

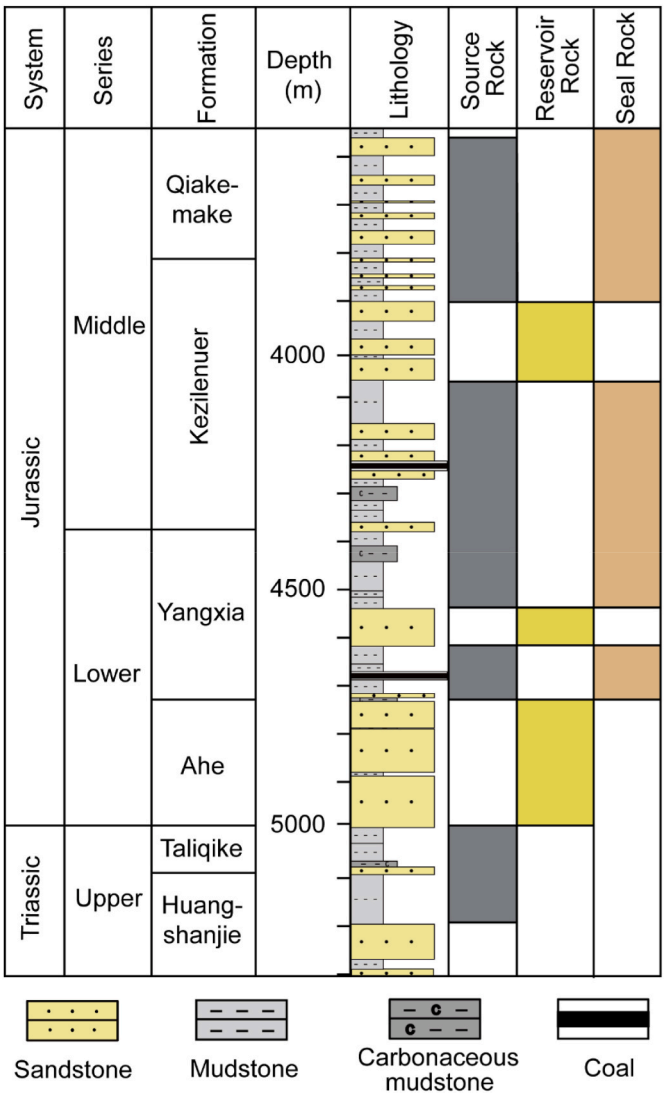

Fig. 2. Generalized Upper Triassic to Middle Jurassic stratigraphy of the YN-2 well in the Kuqa foreland basin (see Fig. 1c for well location), showing lithofacies and multiple source, reservoir, and seal layers (modified from Li et al., 2019).

with similar organic matters. Although it is a common practice to use default kinetics in the basin modeling program based on kerogen types (Waples et al., 1992; Pepper and Corvi, 1995), customized kinetics for individual source rocks (kerogen) in a study area are necessary for accurately simulating hydrocarbon generation (Ungerer, 1990; Dieckmann, 2005; Peters et al., 2015).

The Kuqa foreland basin in the northern part of the Tarim Basin, NW China, is rich in oil and gas resources, especially gas (Zhao and Zhang, 2002; He et al., 2013; Yang et al., 2021). To date, several large to giant gas fields have been discovered, mainly in the Kelasu (e.g. Kela-2, Dabei-1 and Bozi-9 gas fields), the Qiulitage (e.g. Zhongqiu-1 and Dina-2 gas fields), and the Northern structural belts (e.g., Dibei and Tudong-2 gas fields) (Lu et al., 2012; Tian et al., 2020; Tang et al., 2021). Multiple layers of source rocks were developed in the Upper Triassic and Lower to Middle Jurassic stratigraphic intervals, providing a significant material base for oil and gas accumulations (Tang et al., 2021). These source rocks, which were developed in various depositional environments within a fluvial-lacustrine system, can be divided into three categories: dark mudstone, carbonaceous mudstone, and coal (Li et al., 2019). Little systematic work has been done to investigate the petroleum generation and cracking characteristics and kinetics of these source rocks based on pyrolysis simulation experiments. Li et al. (2004, 2005) for the first time studied the methane generative kinetics of the mudstone, carbonaceous mudstone, and coal source rocks in the area based on sealed gold tube pyrolysis experiments, but the maturities of their samples were too high (0.88%–1.05% Ro). Zou et al. (2006) and Huang et al. (2019) only investigated the gas or oil and gas generative characteristics and kinetics of coal. It is difficult to compare the generative abilities and the generation and cracking kinetics among the three types of source rock. Such information is crucial for assessing source rocks, reconstructing oil and gas generation and cracking processes, and calculating oil and gas resources, etc. In this study, three immature mudstone, carbonaceous mudstone and coal source rock samples in the Kuqa foreland basin are selected to conduct closed-system pyrolysis simulation experiments.

Two kinds of physical experiments are usually chosen to depict the evolutional processes and kinetics of oil and gas from kerogen decomposition, which are open-system pyrolysis (Braun and Burnham, 1987; Vyazovkin and Wight, 1999; Vyazovkin et al., 2011) and closed-system pyrolysis, including hydrous pyrolysis (Lewan and Ruble, 2002), microscale sealed vessel pyrolysis (Horsfield et al., 1989) and sealed gold tube pyrolysis (Behar et al., 1992). Although debates have been ongoing regarding the reliability of kinetics determined from these two approaches (Schenk and Horsfield, 1993; Ritter et al., 1995; Barth et al., 1996; Lewan and Ruble, 2002), there is a general consensus that closed-system pyrolysis is preferred to investigate both the generation and cracking processes of source rocks.

The aims of this study are to: (1) determine oil and gas yields from the mudstone, carbonaceous mudstone, and coal source rocks based on sealed gold tube pyrolysis; (2) calculate both the generation and cracking kinetic parameters of the three source rocks; (3) compare oil and gas generation and cracking processes among the source rocks; and (4) reconstruct the oil and gas generation and cracking during the geological evolution in the Kuqa foreland basin.

2. Geological setting

Located in northwestern China (Fig. 1a), the Tarim Basin is the largest onshore petroliferous basin in China (Tian et al., 2021). The Kuqa foreland basin is located in the northern margin of the Tarim Basin and covers an area of approximately 28,000 km^2 with maximum east-west and south to north dimensions of approximately 550 km and 120 km, respectively (Fig. 1b; Jin et al., 2008; Zhang et al., 2011). Developed on a Permian basement, the Kuqa foreland basin is interpreted as a peripheral foreland basin (Jia, 1992; Tian et al., 1996) or a collisional successor foreland basin (Hendrix et al., 1992; Graham et al., 1993). The basin has experienced three stages of tectonic evolution, including a foreland basin stage during the late Permian to the Triassic, an extensional rift stage from the late Triassic to the middle Jurassic, and a rejuvenated foreland basin stage since the Neogene (Graham et al., 1993). The basin comprises four structural belts and three sags, namely the Northern monocline belt, the Kelasu and Qiulitage fold-and-thrust belts, and the Southern Slope from north to south, with the Wushi, Baicheng, and Yangxia sags developed in-between the structural belts from west to east, respectively (Fig. 1c).

The Kuqa foreland basin is filled with Mesozoic and Cenozoic sediments, with a maximum thickness of over 10,000 m, mainly in depocenters of the Baicheng and Yangxia sags (Fig. 1c and d). The Mesozoic succession was deposited in lacustrine-fluvial settings, consisting of sandstones, mudstones and some coal seams, and has an average thickness of 2000–3000 m (Jia et al., 2002). The Triassic and Jurassic strata are thin to absence in the Southern Slope area (Fig. 1d). During the Neogene, the entire basin underwent a rapid subsidence and was accompanied by the deposition of 3000–5000 m of lacustrine and fluvial sediments (Jia et al., 2002). Affected by the late Himalayan orogeny, the basin was compressed strongly along the N–S direction and the northern part of the basin was uplifted, resulting in a major unconformity in the

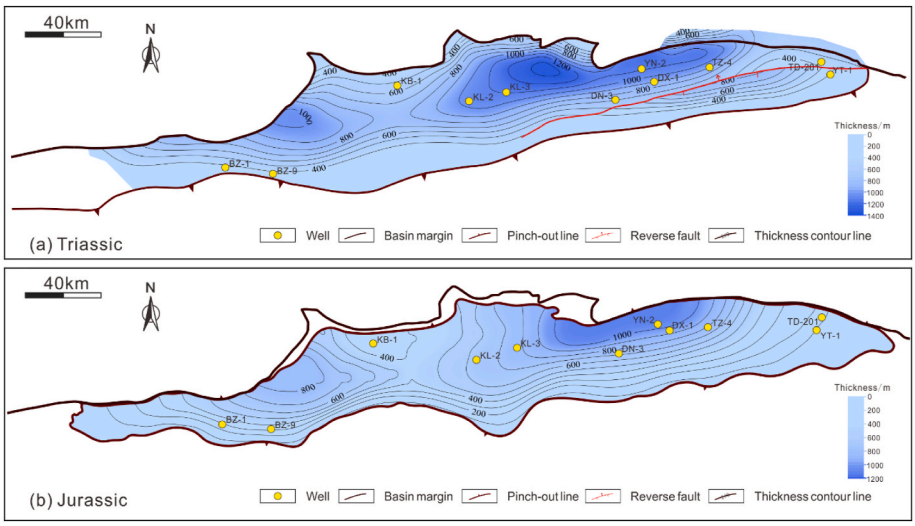

Fig. 3. Thickness distributions of the Triassic (a) and Jurassic (b) source rocks, showing generally thick and wide occurrence of the two sets of source rocks (modified from Tang et al., 2021).

Table 1
Sample information of the three types of source rock investigated. C-Mudstone = Carbonaceous Mudstone; Fm. = Formation.

Fm.	Depth (m)	Lithology	TOC (wt. %)	S_1 (mg HC/g)	S_2 (mg HC/g)	S_3 (mg CO_2/g)	T_{max} (°C)	HI (mg HC/g TOC)	OI (mg CO_2/g TOC)	H/C	O/C	Ro (%)
J_2kz	419.50	Mudstone	5.78	0.21	8.00	1.09	424.5	138.4	19	1.09	0.20	0.46
J_1y	608.56	C-Mudstone	28.31	0.63	31.52	3.99	426.0	111.3	14	0.84	0.14	0.53
J_1y	608.26	Coal	69.08	2.40	147.31	13.10	426.0	213.2	19	0.81	0.19	0.50

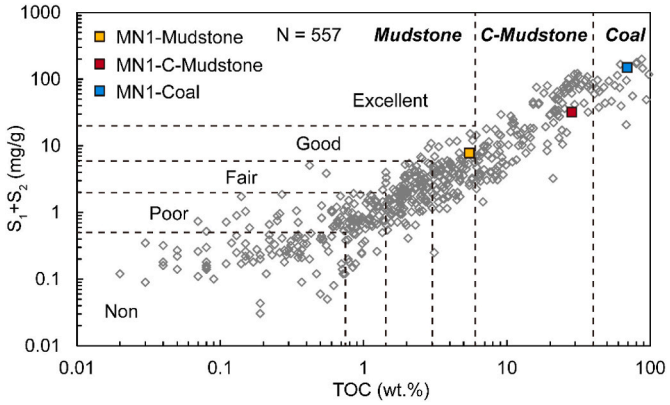

Fig. 4. Plot of TOC versus S_1+S_2 data from source rocks in the eastern part of the Kuqa foreland basin, showing an overall good positive correlation over a wide range. The source rock quality subdivision criterion is based on Chen et al. (1997).

late Pliocene with the removal of several hundred to over 2000 m of sediments due to erosion (Jia et al., 2004).

A total of five sets of source rocks were developed in the Upper Triassic to the Middle Jurassic in the Kuqa foreland basin including an oil-prone lacustrine mudstones deposited in shallow to semi-deep lacustrine settings as represented by the Upper Triassic Huangshanjie and Middle Jurassic Qiakemake formations, and gas-prone coaly source rocks of paludal to lacustrine settings as represented by the Upper Triassic Taliqike, Lower Jurassic Yangxia and Middle Jurassic Kezilenuer formations (Fig. 2). Both Triassic and Jurassic source rocks are thick (mostly >400 m) and distributed widely. The depocenters of source rocks are beneath the current Northern and Kelasu structural

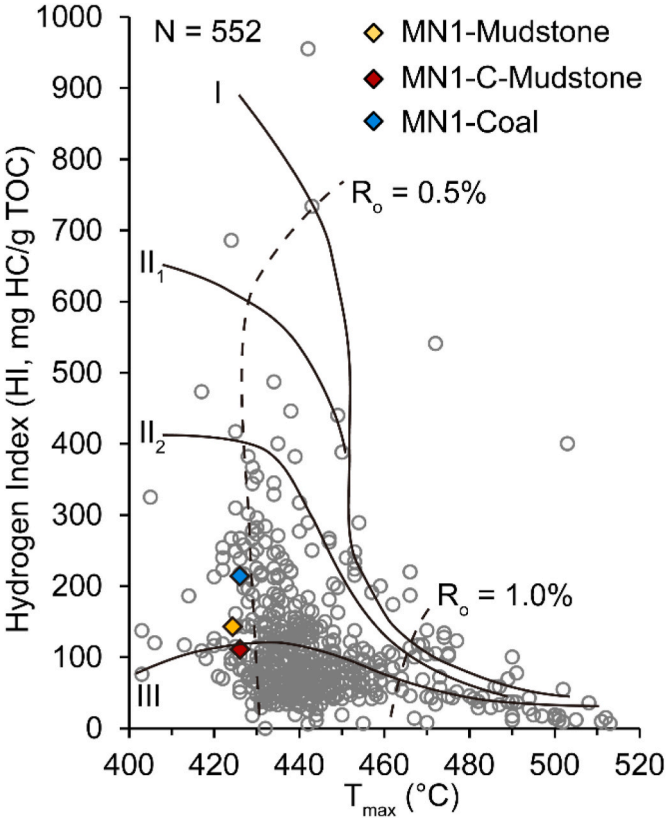

Fig. 5. Plot of T_{max} and hydrogen index (HI) of source rocks from the eastern part of the Kuqa foreland basin, showing typical Type II_2 and Type III kerogens.

Table 2
Compositions of liquid and gaseous hydrocarbons, and inorganic gases generated from pyrolysis experiments for the mudstone, carbonaceous mudstone and coal source rocks. Temp. = Temperature. Easy Ro% values were calculated according to Sweeney and Burnham (1990).

Temp. (°C)	Easy Ro%	C_1 (mg/g TOC)	C_2 (mg/g TOC)	C_3 (mg/g TOC)	C_4 (mg/g TOC)	C_5 (mg/g TOC)	C_2–C_5 (mg/g TOC)	C_1/(C_1–C_5)	CO_2 (mg/g TOC)	H_2 (mg/g TOC)	H_2S (mg/g TOC)	C_6–C_{14} (mg/g TOC)	C_{15+} (mg/g TOC)
Mudstone, heating rate = 20 °C/h													
336	0.57	0.49	0.12	0.09	0.03	0.00	0.25	0.66	67.38	0.00	0.00	0.45	2.44
360	0.68	0.70	0.21	0.18	0.05	0.00	0.45	0.61	77.53	0.00	0.00	1.70	5.17
384	0.79	1.30	0.60	0.47	0.13	0.01	1.21	0.52	95.94	0.01	0.00	2.31	7.60
408	0.96	2.92	1.64	0.93	0.20	0.02	2.79	0.51	117.12	0.03	0.26	5.08	17.48
432	1.19	6.70	3.29	1.29	0.21	0.02	4.81	0.58	139.61	0.06	0.45	6.50	13.19
456	1.47	15.21	4.73	1.15	0.14	0.01	6.03	0.72	143.46	0.11	0.38	10.59	8.23
480	1.81	27.75	5.09	0.65	0.05	0.00	5.79	0.83	158.19	0.16	0.35	9.22	6.72
504	2.19	43.36	3.20	0.17	0.01	0.00	3.37	0.93	158.24	0.26	0.31	8.22	3.45
528	2.62	51.69	2.61	0.14	0.00	0.00	2.75	0.95	170.76	0.34	0.35	7.53	0.00
552	3.06	62.61	1.32	0.02	0.00	0.00	1.34	0.98	188.32	0.42	0.44	5.78	0.00
576	3.50	74.02	0.97	0.01	0.00	0.00	0.99	0.99	198.68	0.60	0.49	5.56	0.00
600	3.87	90.13	0.92	0.00	0.00	0.00	0.92	0.99	222.92	0.82	0.66	4.85	0.00
Mudstone, heating rate = 2 °C/h													
336	0.73	1.11	0.41	0.30	0.07	0.01	0.79	0.58	120.98	0.00	0.00	2.94	14.91
360	0.86	2.00	1.03	0.59	0.12	0.01	1.75	0.53	116.23	0.01	0.13	5.82	19.79
384	1.08	4.71	2.47	0.99	0.16	0.02	3.63	0.56	138.62	0.02	0.22	8.06	11.37
408	1.36	10.87	4.19	1.04	0.12	0.01	5.36	0.67	151.91	0.05	0.29	12.49	9.47
432	1.69	23.72	4.84	0.59	0.05	0.00	5.48	0.81	161.73	0.08	0.27	10.51	7.37
456	2.09	36.30	4.10	0.21	0.01	0.00	4.32	0.89	171.16	0.12	0.26	8.30	5.02
480	2.52	52.41	1.95	0.04	0.00	0.00	1.99	0.96	176.20	0.19	0.26	7.76	2.62
504	2.99	64.83	0.99	0.02	0.00	0.00	1.01	0.98	182.26	0.28	0.31	7.18	0.00
528	3.46	81.17	0.78	0.01	0.00	0.00	0.80	0.99	209.94	0.41	0.46	5.81	0.00
552	3.86	96.41	0.65	0.01	0.00	0.00	0.66	0.99	236.42	0.56	0.60	3.81	0.00
576	4.19	121.08	0.39	0.00	0.00	0.00	0.39	1.00	275.85	0.80	0.89	1.47	0.00
600	4.45	138.17	0.14	0.00	0.00	0.00	0.14	1.00	310.34	1.00	1.12	0.30	0.00
C-Mudstone, heating rate = 20 °C/h													
336	0.57	0.20	0.03	0.01	0.00	0.00	0.04	0.85	29.47	0.00	0.00	0.20	2.18
360	0.68	0.45	0.09	0.02	0.00	0.00	0.11	0.80	52.52	0.00	0.00	0.45	4.36
384	0.79	0.75	0.24	0.07	0.01	0.00	0.32	0.70	59.83	0.00	0.00	0.99	6.60
408	0.96	1.83	0.65	0.14	0.02	0.00	0.81	0.69	72.59	0.02	0.00	2.02	9.10
432	1.19	2.98	0.92	0.16	0.03	0.00	1.11	0.73	75.69	0.02	0.00	2.65	4.56
456	1.47	11.43	1.96	0.19	0.02	0.00	2.17	0.84	100.44	0.06	0.00	3.12	2.45
480	1.81	19.90	1.74	0.10	0.01	0.00	1.85	0.91	98.83	0.10	0.00	3.66	2.56
504	2.19	32.70	1.04	0.03	0.00	0.00	1.07	0.97	107.49	0.17	0.00	4.67	0.00
528	2.62	42.56	0.93	0.03	0.00	0.00	0.95	0.98	124.11	0.21	0.00	5.55	0.00
552	3.06	49.58	0.60	0.01	0.00	0.00	0.60	0.99	126.72	0.28	0.00	5.19	0.00
576	3.50	58.14	0.61	0.00	0.00	0.00	0.61	0.99	133.66	0.38	0.00	4.05	0.00
600	3.87	72.25	0.44	0.00	0.00	0.00	0.44	0.99	150.03	0.51	0.00	2.61	0.00
C-Mudstone, heating rate = 2 °C/h													
336	0.73	0.57	0.17	0.05	0.01	0.00	0.23	0.71	71.93	0.00	0.00	1.20	4.18
360	0.86	1.15	0.38	0.08	0.01	0.00	0.47	0.71	69.89	0.00	0.00	1.85	8.74
384	1.08	2.84	0.89	0.19	0.04	0.00	1.13	0.72	79.49	0.01	0.00	3.24	11.32
408	1.36	6.78	1.43	0.23	0.04	0.00	1.70	0.80	84.94	0.03	0.00	3.91	9.32
432	1.69	15.21	1.69	0.16	0.02	0.00	1.88	0.89	92.22	0.03	0.00	5.16	7.25
456	2.09	22.87	1.22	0.04	0.00	0.00	1.27	0.95	88.44	0.07	0.00	5.59	5.08
480	2.52	37.80	0.71	0.02	0.00	0.00	0.72	0.98	115.52	0.12	0.00	4.47	5.15
504	2.99	55.28	0.55	0.01	0.00	0.00	0.56	0.99	145.74	0.20	0.00	4.18	2.93
528	3.46	65.15	0.42	0.01	0.00	0.00	0.43	0.99	144.74	0.27	0.00	3.10	0.00
552	3.86	81.86	0.33	0.00	0.00	0.00	0.33	1.00	172.82	0.36	0.00	2.35	0.00
576	4.19	99.78	0.20	0.00	0.00	0.00	0.20	1.00	193.81	0.49	0.00	1.22	0.00
600	4.45	108.77	0.15	0.00	0.00	0.00	0.15	1.00	204.78	0.62	0.00	0.91	0.00
Coal, heating rate = 20 °C/h													
336	0.57	0.42	0.11	0.05	0.01	0.00	0.17	0.71	30.64	0.00	0.00	0.34	2.19
360	0.68	0.91	0.30	0.14	0.04	0.01	0.49	0.65	47.56	0.00	0.00	0.55	8.83
384	0.79	1.89	1.00	0.58	0.22	0.07	1.87	0.50	61.53	0.01	0.13	1.22	22.97
408	0.96	4.11	2.70	1.49	0.59	0.21	4.99	0.45	65.96	0.02	0.18	3.56	34.72
432	1.19	9.01	5.68	2.84	1.02	0.36	9.91	0.48	80.60	0.05	0.40	7.10	27.94
456	1.47	18.49	8.87	3.62	1.09	0.26	13.84	0.57	85.71	0.09	0.58	7.06	11.37
480	1.81	31.07	10.38	3.01	0.79	0.10	14.28	0.69	90.65	0.13	0.51	5.44	2.63
504	2.19	49.84	8.46	1.16	0.16	0.01	9.78	0.84	96.40	0.23	0.33	4.30	0.00
528	2.62	62.39	5.64	0.27	0.02	0.00	5.93	0.91	104.31	0.28	0.34	5.30	0.00
552	3.06	71.99	3.65	0.09	0.00	0.00	3.74	0.95	109.81	0.34	0.39	5.29	0.00
576	3.50	81.51	1.84	0.02	0.00	0.00	1.85	0.98	116.66	0.44	0.43	3.85	0.00
600	3.87	92.01	1.01	0.00	0.00	0.00	1.01	0.99	126.61	0.56	0.48	2.55	0.00
Coal, heating rate = 2 °C/h													
336	0.73	1.48	0.63	0.30	0.09	0.02	1.05	0.59	64.09	0.00	0.00	1.54	12.65
360	0.86	2.96	1.77	0.86	0.21	0.04	2.87	0.51	72.95	0.01	0.10	3.71	27.87
384	1.08	6.45	4.16	1.88	0.47	0.10	6.61	0.49	80.81	0.02	0.25	5.01	32.11
408	1.36	13.14	7.01	3.34	1.27	0.46	12.07	0.52	95.03	0.04	0.37	7.78	11.55
432	1.69	26.50	10.29	3.02	0.63	0.10	14.03	0.65	98.09	0.07	0.48	8.04	2.38

(*continued on next page*)

Table 2 (*continued*)

Temp. (°C)	Easy Ro%	C_1 (mg/g TOC)	C_2 (mg/g TOC)	C_3 (mg/g TOC)	C_4 (mg/g TOC)	C_5 (mg/g TOC)	C_2–C_5 (mg/g TOC)	C_1/(C_1–C_5)	CO_2 (mg/g TOC)	H_2 (mg/g TOC)	H_2S (mg/g TOC)	C_6–C_{14} (mg/g TOC)	C_{15+} (mg/g TOC)
456	2.09	41.01	10.17	1.88	0.37	0.02	12.43	0.77	100.32	0.11	0.41	6.21	0.00
480	2.52	60.22	6.81	0.39	0.03	0.00	7.23	0.89	107.34	0.17	0.35	5.35	0.00
504	2.99	73.28	2.52	0.05	0.00	0.00	2.57	0.97	110.40	0.24	0.25	3.98	0.00
528	3.46	87.05	0.87	0.01	0.00	0.00	0.88	0.99	123.42	0.31	0.25	3.33	0.00
552	3.86	98.07	0.53	0.01	0.00	0.00	0.54	0.99	136.88	0.39	0.27	2.32	0.00
576	4.19	111.30	0.32	0.00	0.00	0.00	0.32	1.00	154.70	0.52	0.59	0.95	0.00
600	4.45	120.56	0.22	0.00	0.00	0.00	0.22	1.00	165.45	0.65	0.82	0.84	0.00

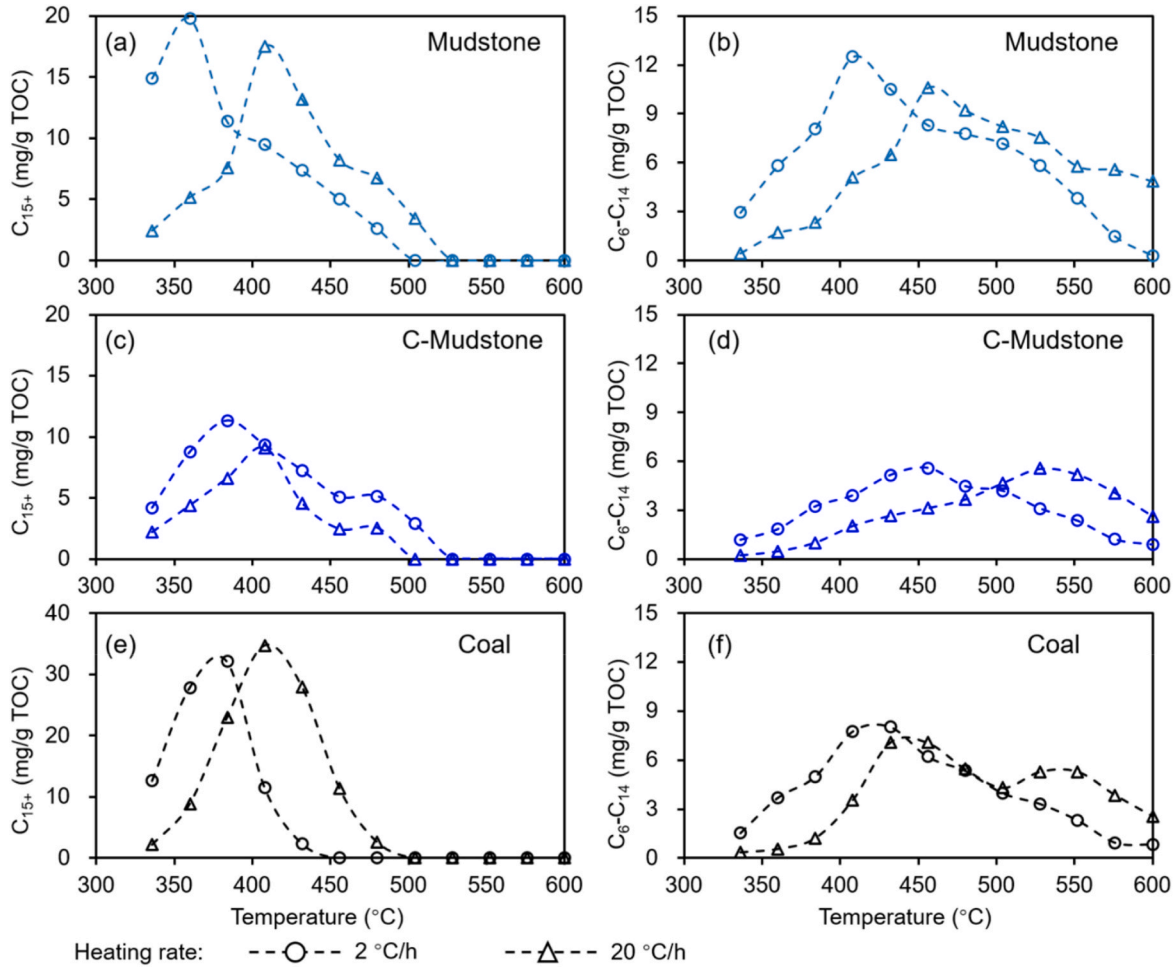

Fig. 6. Heavy (C_{15+} components) and light to medium (C_6–C_{14} components) liquid hydrocarbon yields at each pyrolytic temperature under 2 °C/h and 20 °C/h heating rates for the Kuqa foreland basin mudstone (a, b), carbonaceous mudstone (c, d), and coal (e, f) source rocks.

belts, with a maximum thickness of over 1000 m for both of the Triassic and Jurassic source rocks, which pinch out towards to the south and north (Fig. 3; Tang et al., 2021). Thick and tightly-cemented sandstones primarily developed in the Lower Jurassic Ahe Formation, having been proved to be the main gas-bearing layer in the Northern structural belt. Several thin sandstone layers are also present in the Yangxia and Kezilenuer formations. These sandstones are intermingled with mudstones, forming several favorable source-reservoir-seal assemblages (Fig. 2).

3. Samples and methods

3.1. Samples

Three shallow burial source rock samples were collected from the Lower Jurassic Yangxia and the Middle Jurassic Kezilenuer formations in the Mingnan-1 well (MN-1 in Fig. 1c) in northeastern part of the Kuqa foreland basin. The three samples include a mudstone sample at 419.5 m, a coal sample at 608.26 m, and a carbonaceous mudstone sample at 608.56 m, respectively. They were subject to thermal pyrolysis with the pyrolysis products being analyzed by GC-MS and GC-IRMS.

3.2. Rock-Eval pyrolysis

Three source rock samples were measured for Rock-Eval pyrolysis using a Rock-Eval VI instrument following the procedure of Espitalié et al. (1977) and Peters (1986). About 100 mg of rock sample was used for measurement. The samples were pyrolyzed between 300 and 650 °C under an inert atmosphere of nitrogen. Parameters measured include Total Organic Carbon (TOC), free and absorbed hydrocarbons (S_1), remaining hydrocarbon generative potential in mg HC/g rock (S_2), the

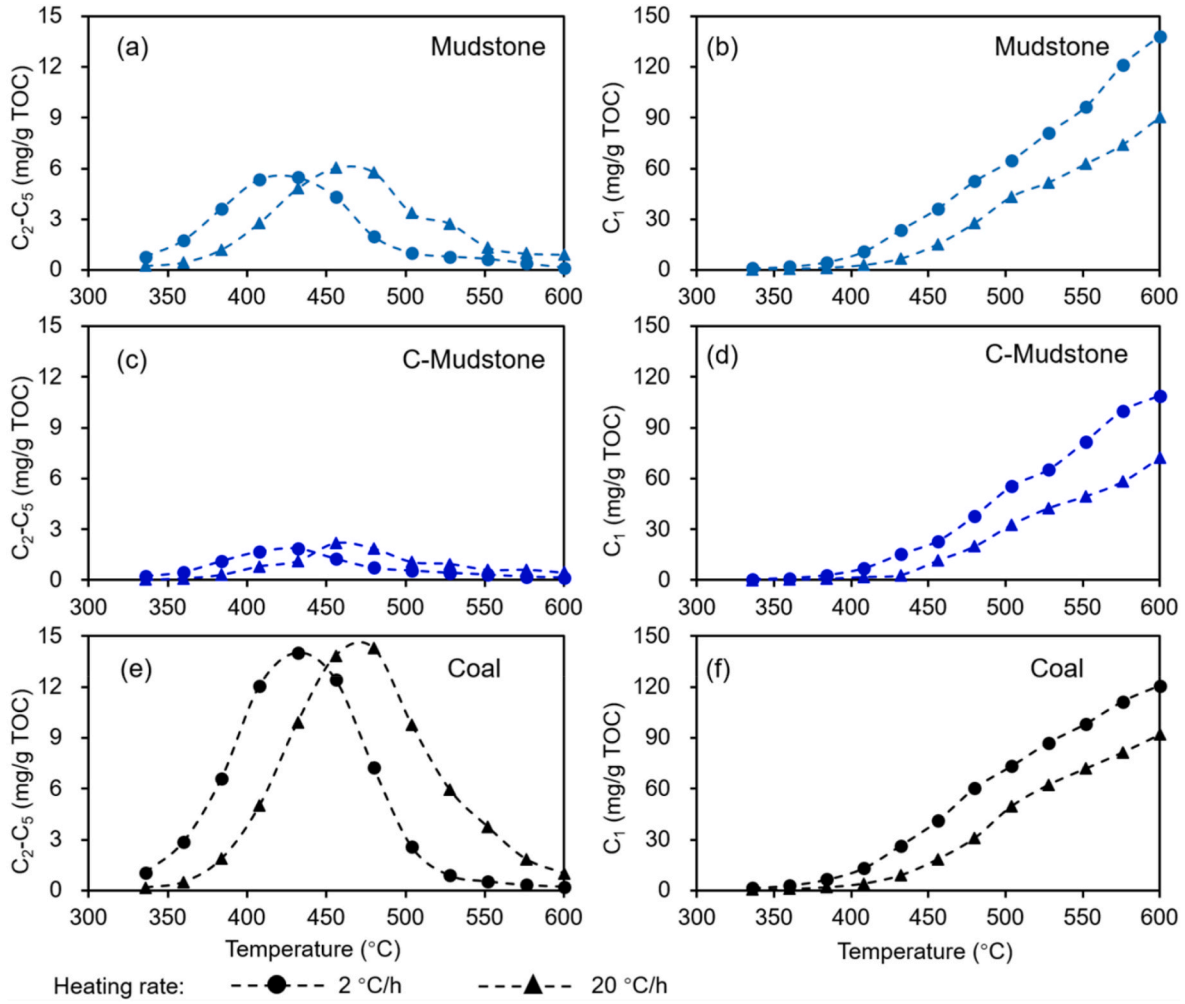

Fig. 7. Wet gases (C_2–C_5) and methane yields for the mudstone (a, b), carbonaceous mudstone (c, d), and coal (e, f) source rocks at each pyrolytic temperature under 2 °C/h and 20 °C/h heating rates, respectively.

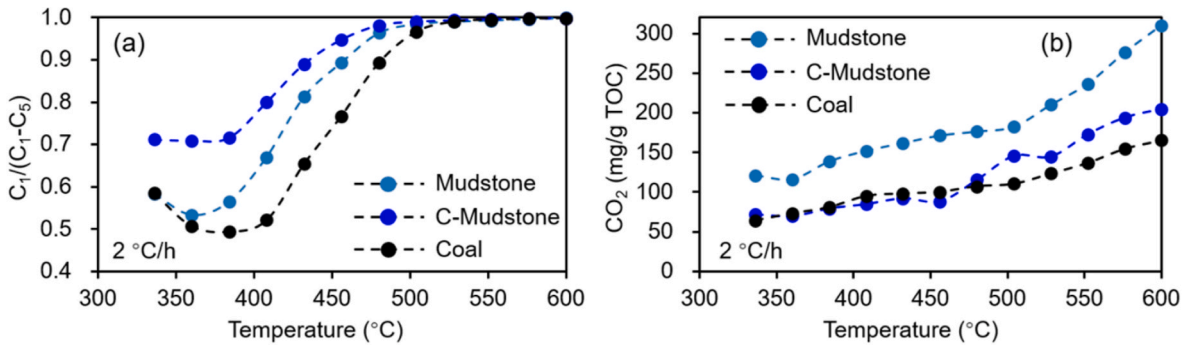

Fig. 8. Dryness index of hydrocarbon gases (a) and CO_2 yields (b) at each temperature under a 2 °C/h heating rate for the mudstone, carbonaceous mudstone, and coal source rocks.

quantity of CO_2 produced from pyrolysis of the organic matter up to a temperature of 390 °C in mg CO_2/g rock (S_3), and the temperature corresponding to the maximum pyrolysis yield (T_{max}). Hydrogen index (HI) and oxygen index (OI) were then calculated based on these results.

3.3. Vitrinite reflectance

Vitrinite reflectances (Ro%) were measured for the three source rock samples using a MPV-SP microphotometer. Polished sections were firstly made using the standard procedure of Taylor et al. (1998) for Ro analysis. Approximately 100 points per sample were analyzed at random orientations using a Zeiss Yttrium-Aluminium- Garnet (R = 0.889%) as a reference standard.

3.4. Sealed gold tube pyrolysis experiment

A sealed gold tube pyrolysis approach was employed in this study to investigate oil and gas generation and cracking yields of the three

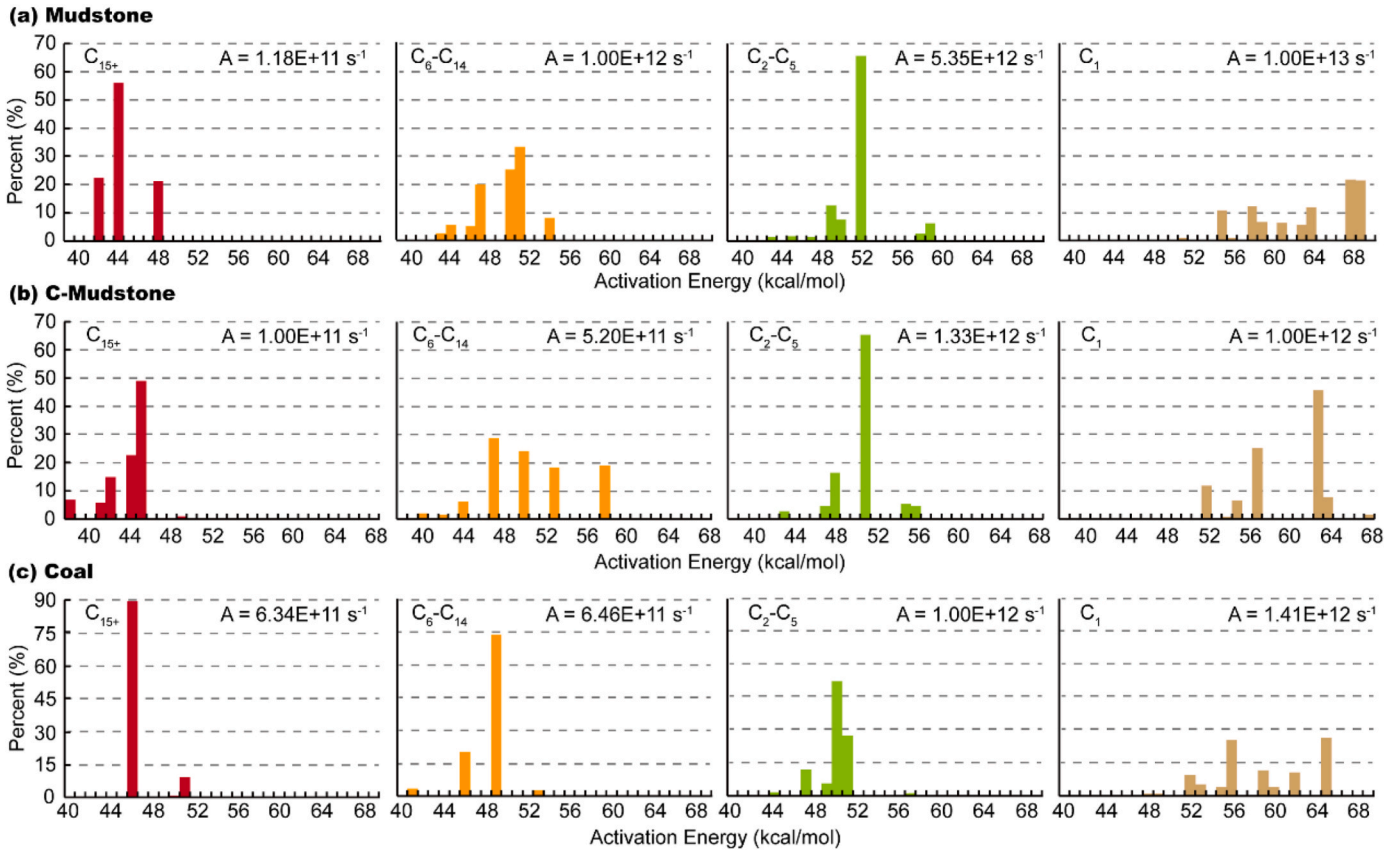

Fig. 9. Generative kinetic parameters of C_{15+}, C_6–C_{14}, C_2–C_5 and methane for mudstone (a), carbonaceous mudstone (b) and coal (c) samples in the Kuqa foreland basin. Parameter A is the frequency factor.

immature source rock samples. Kerogen was first isolated from each sample (Jasper et al., 2009). Approximate 20–80 mg of homogenized fine powder kerogens from each sample was prepared. The powdered kerogen sample was then loaded into individual gold capsules following the general principle that the higher the final pyrolysis temperatures are, the less material would be required. The gold capsule is 50 mm long, and has an inner diameter of 5 mm and a wall thickness of 0.25 mm. Gold capsules were first welded at one end and heated to 800 °C for 3 h to remove any potential residual organic materials, and were then loaded with samples. After loading kerogen powders, gold capsules were purged with argon gas to remove air and were then welded at the open end while the other end is submerged in cold water to avoid damage to the sample during high-temperature welding (Lu et al., 2011). The sealed gold tubes were firstly submerged into hot water (~80 °C) for leak detection, and were then placed in stainless steel pressure vessels and heated in a furnace. The internal pressure of the vessels was kept at 50 MPa (±0.1 MPa) by using pressurized water. Two heating rates, 2 °C/h and 20 °C/h, were applied. For each heating rate, the vessels were heated from room temperature to 250 °C in 10 h and then heated to the designated temperatures at the designated heating rate with an accuracy of less than ±1 °C. At each heating rate, 12 temperature points ranging from 336 °C to 600 °C were programmed for each source rock. After reaching the target temperature, each vessel was taken out and quenched to room temperature in cold water within 10 min.

Gas components were first collected and analyzed from the pyrolytic gold capsules. All gases yielded were collected by piercing gold tubes under vacuum and gathered and quantitatively analyzed through a connected Agilent 6890 GC modified by Wasson ECE Instrumentation. The GC oven temperature was held at 50 °C for 5 min before ramping to 130 °C at a heating rate of 15 °C/min and finally reaching to 180 °C at a heating rate of 25 °C/min and held for 4 min. The Agilent 6890 GC uses an external standard and has a relative analytical error of less than 0.5%.

After detection of gas components, each capsule was then cooled in liquid nitrogen for 5 min and cut swiftly into several pieces and put into an 8 ml vial with 2 ml of cold solvent of *n*-pentane (Pan et al., 2009; Li et al., 2016). The C_6–C_{14} hydrocarbon components were ultrasonically extracted for 5 min, 3 times, and then settled for 72 h to allow the pentane solutions to settle. Deuterated *n*-C_{24} was added to vails as an internal standard for quantification. The pentane solution was then analyzed using an HP6890 GC with an FID detector. The oven temperature was kept at 40 °C for 20 min, and then raised to 120 °C at a heating rate of 4 °C/min, and then increased to 290 °C at a heating rate of 3 °C/min, and finally held at 290 °C for 25 min. The liquid hydrocarbons were dried and weighted three times until obtaining a constant weight (±1 mg), which was recorded as the C_{15+} yield (Wang et al., 2021).

3.5. Kinetic analysis

Organic matter undergoes thermal cracking to generate hydrocarbons at rates that are dependent on temperature. This can be expressed by the first-order kinetic reaction: dC/dt = -kC, where C is the fraction of organic matter unreacted into hydrocarbons, t is time, and k is the rate constant following the Arrhenius law, i.e., k varies with temperature according to:

$$k = Ae^{\frac{-E}{RT(t)}}$$

where, A is the frequency factor (s^{-1}), e is the mathematical constant (= 2.7183), E is the activation energy (kcal/mol), R is the gas constant (= 0.001987 kcal/mol/K), and T is the absolute temperature, which is a function of time (t) (Zhang et al., 2008). Kinetic parameters including E and A for the generation and cracking of hydrocarbon components were derived from the pyrolysis data using the *Kinetics 1998* program (Braun

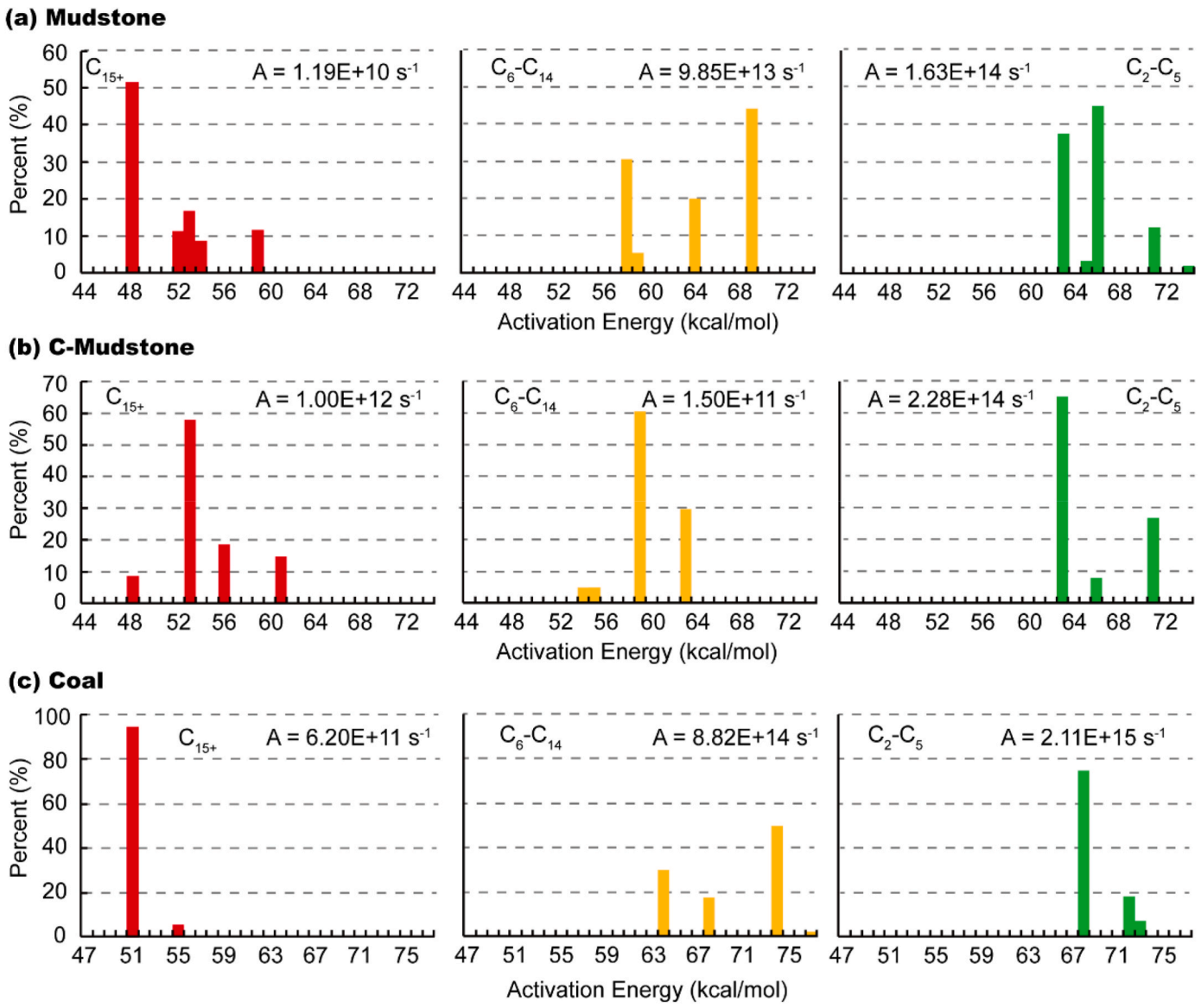

Fig. 10. Kinetic parameters for cracking C_{15+}, C_6–C_{14} and C_2–C_5 components for the mudstone (a), carbonaceous mudstone (b) and coal (c) samples in the Kuqa foreland basin.

and Burnham, 1987). It can fit rate parameters to chemical reaction data measured at a series of constant temperatures and constant heating rates. The discrete distribution model fits an average frequency factor and relative fractions and activation energies for up to 25 parallel, first-order reactions. Once convergence is reached by the discrete model, the parameter space is further systematically searched to achieve a global convergence (Braun and Burnham, 1994; Burnham and Braun, 1999). A discrete distribution of activation energies at 1-kcal/mol intervals with a single frequency factor can finally be fitted for each of the sample.

3.6. One-dimensional basin modeling

One-dimensional (1D) basin modeling was carried out on the actual YN-2 well and another pseudo well (PW-1), which are located on the northern slope and near the depocenter of the Kuqa foreland basin, respectively (Fig. 1d), using the Schlumberger PetroMod 2017 software. The main principle and procedure of the modeling are detailed in Hantschel and Kauerauf (2009). The lithology and depth inputs for the YN-2 well and PW-1 came from the drilling info and the 2D cross-section derived from seismic interpretation, respectively. The ages of each stratigraphic interval were taken from Jin (2005) and the International Chronostratigraphic Chart 2021 (www.stratigraphy.org). Eroded thicknesses during the late Jurassic, late Cretaceous, and late Pliocene orogenic phases were assigned according to Liu et al. (2018). Heat flow values in the eastern part of the Kuqa foreland basin are taken from Wang et al. (2003) and Liu et al. (2016, 2018). Paleo-water depths were estimated from the sequence stratigraphic architecture and sedimentary facies characteristics. Sediment-water-interface temperatures (SWITs) were calculated using an integrated PetroMod module based on Wygrala (1989), which provides a global surface temperature versus time curve based on the latitude of the study area. Herein, the Kuqa foreland basin is presently located at approximately 41°N.

4. Results

4.1. Geochemical characteristics and representativeness of the three samples

Rock-Eval pyrolysis and vitrinite reflectance (Ro%) measurements

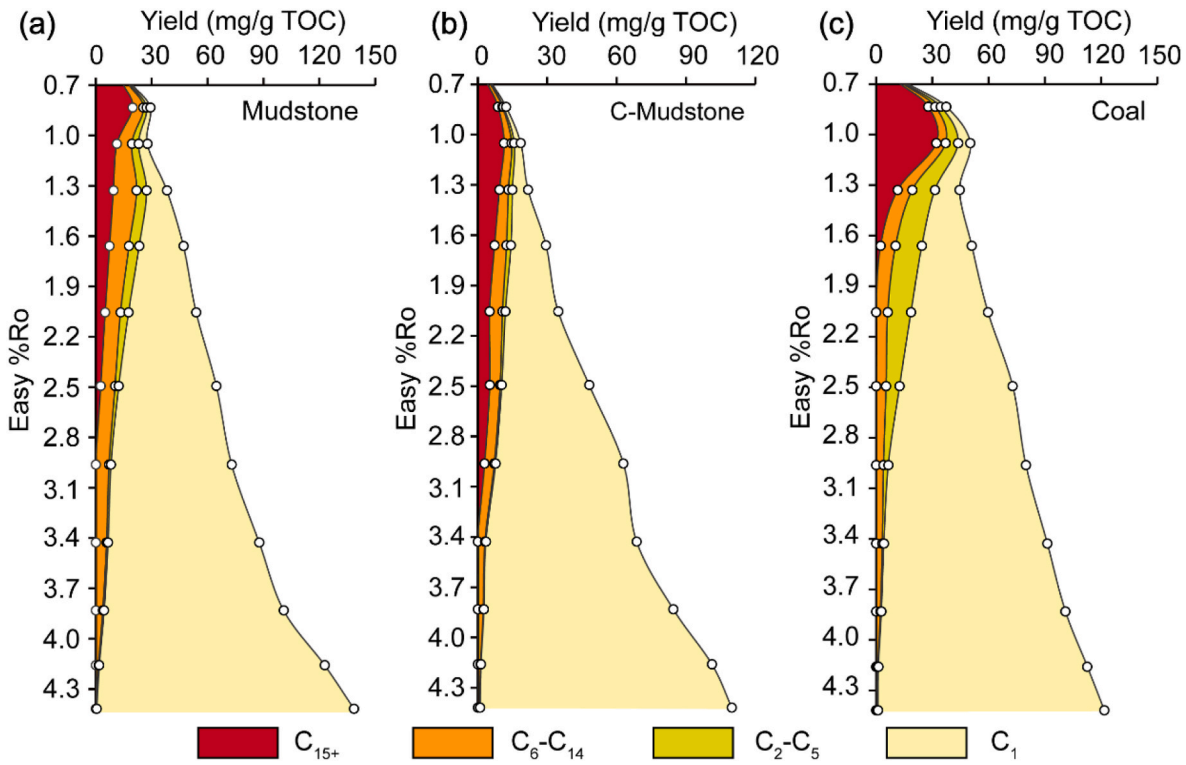

Fig. 11. Hydrocarbon generation evolution of the mudstone (a), carbonaceous mudstone (b), and coal (c) samples from the Kuqa foreland basin, expressed as yields individual hydrocarbon components and Easy%Ro at a heating rate of 2 °C/h.

were carried out (Table 1). The TOC values of the mudstone, carbonaceous mudstone and coal source rock samples are 5.78 wt%, 28.31 wt% and 69.08 wt%, respectively, which are comparable to the subdivision criteria for coaly source rocks proposed by Chen et al. (1997) for mudstone (TOC <6 wt%), carbonaceous mudstone (TOC: 6 wt%–40 wt %) and coal (TOC >40 wt%). This subdivision criterion was developed based on the analysis of over 2300 source rock samples from Jurassic coaly strata in northwestern China (Chen et al., 1997), and is thus appropriate for use in this study. The measured Ro% values of the mudstone, carbonaceous mudstone, and coal are 0.46%, 0.53%, and 0.50%, respectively, all belonging to an immature hydrocarbon generation stage (Sweeney and Burnham, 1990). The source rock samples are thus suitable for pyrolysis simulation experiments.

To ensure the selected source samples are representative of the three types of source rocks in the eastern part of the Kuqa foreland basin, we collected over 550 measured source rock geochemical data within the Triassic and Jurassic intervals from 22 wells and outcrops in the eastern part of the basin (data supplied by the Tarim Oilfield Company, PetroChina). The TOC and S_1+S_2 values display a good positive relationship and show broad ranges among all of the mudstone, carbonaceous mudstone, and coal source rocks. Mudstones in this area generally belong to fair to good source rocks. The three samples from the MN-1 well represent a good-quality mudstone, a fair-to good-quality carbonaceous mudstone, and a fair-quality coal among the source rocks in the eastern part of the Kuqa basin (Fig. 4). Most of the source rocks in the eastern part of the basin including the selected samples from the MN-1 well are of Type II_2 and Type III kerogen (Fig. 5). Therefore, the immature mudstone, carbonaceous mudstone, and coal source rocks from the MN-1 well are representative of the major source types in the eastern part of the Kuqa foreland basin.

4.2. Hydrocarbon yields of the pyrolytic products

Both liquid and gaseous hydrocarbons, and inorganic gases (e.g., CO_2, H_2 and H_2S) were quantitatively obtained in terms of mg/g TOC from the sealed gold tube pyrolysis experiments on the three source rock samples. The relationships between the pyrolysis yields and temperatures are shown in Table 2 and Figs. 6–8.

4.2.1. Liquid hydrocarbons

Although being identified mainly as Type II_2 and Type III kerogen, all the three source rocks show some liquid hydrocarbon generation abilities (Fig. 6). With increasing pyrolytic temperature, yields of petroleum generally increased to reach peaks and then decreased due to petroleum cracking at high temperatures in the closed pyrolysis system. The temperature corresponding to peak yields of C_{6+} hydrocarbons is relatively smaller for the slower rate of 2 °C/h compared with that for the faster rate of 20 °C/h. Taking the 2 °C/h heating rate as an example, the maximum yields of heavy petroleum (C_{15+} components) are 19.79 mg/g TOC, 11.32 mg/g TOC and 32.11 mg/g TOC for the mudstone, carbonaceous mudstone and coal, respectively (Fig. 6a, c, e), consistent with the hydrogen index rankings of the three samples. The coal source rocks in the Kuqa foreland basin may contribute significantly to oil generation. Based on the pyrolysis experiments under the 2 °C/h heating rate condition, the maximum generation amounts of light to medium oil (C_6–C_{14} components) are 12.49 mg/g TOC, 5.59 mg/g TOC, and 8.04 mg/g TOC for the mudstone, carbonaceous mudstone and coal samples, respectively (Fig. 6b, d, f), showing a relatively smaller amount when compared with the C_{15+} yields for each type of source rock. Under the 2 °C/h heating rate condition, the temperatures at which C_{15+} yields reach their peaks are 360 °C for the mudstone and 384 °C for both carbonaceous mudstone and the coal, which are significantly lower than the temperatures (408–456 °C) corresponding to the yield peaks of C_6–C_{14} components. Comparatively, the mudstone source rock can generate liquid hydrocarbons at the lowest temperature among the three source rocks; coal requires moderately high temperature to generate liquid hydrocarbons; while the carbonaceous mudstone needs the highest temperature among the three source rocks to generate liquid hydrocarbons, especially for the C_6–C_{14} components.

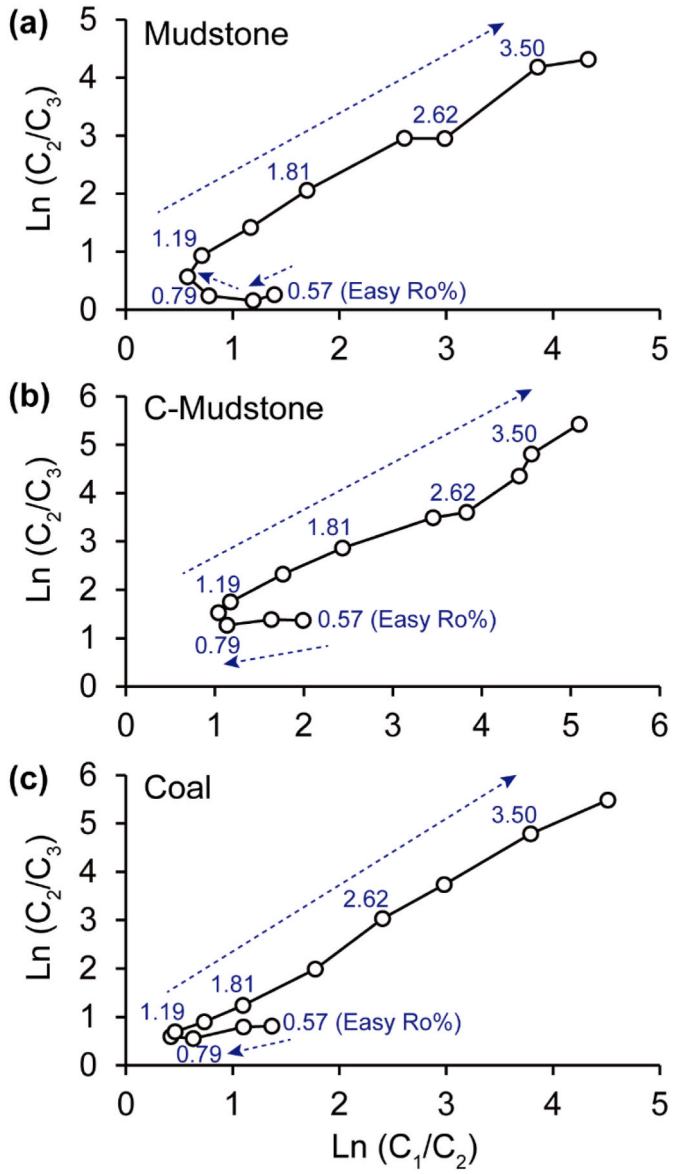

Fig. 12. Plots of Ln (C_1/C_2) versus Ln (C_2/C_3) of the mudstone (a), carbonaceous mudstone (b) and coal (c) samples in the Kuqa foreland basin at a 20 °C/h heating rate.

4.2.2. Gaseous hydrocarbons

Pyrolysis yields of gaseous hydrocarbons including methane and C_2–C_5 components for the three types of source rocks were obtained and then analyzed. Similar to the liquid hydrocarbons, yields of C_2–C_5 components increase to peaks at lower pyrolytic temperatures under the 2 °C/h heating rate condition than under the 20 °C/h heating rate condition for all source rocks. At the 2 °C/h heating rate, the maximum generative amounts of C_2–C_5 components for the mudstone, carbonaceous mudstone and coal source rocks are 5.48 mg/g TOC, 1.88 mg/g TOC, and 14.03 mg/g TOC, respectively (Fig. 7a, c, e), indicating that the coal source rock has nearly 3 times and 7 times of the C_2–C_5 gas generation ability over the mudstone and carbonaceous mudstone. C_2–C_5 gases increase when the pyrolysis temperature is less than 432 °C and start to decrease when the temperature is greater than 432 °C, demonstrating that heavier gases start to crack with increasing temperature within a closed pyrolysis system.

Methane is the final and stable pyrolysis product. For all the three types of source rock, small amounts of methane were initially generated at the beginning of thermal degradation and then increased rapidly with heating (Fig. 7b, d, f). Similar to other closed system pyrolysis studies (e.g., Huss and Burnham, 1982; Behar et al., 1992; Wang et al., 2013), the main accumulation stage of methane occurred after 480 °C for both the 2 °C/h and the 20 °C/h heating rates, because both liquid and heavier gaseous hydrocarbons would start to crack after 480 °C. Methane can be generated from either kerogen thermal degradation or heavier hydrocarbons cracking. The maximum methane yields from the mudstone, carbonaceous mudstone and coal samples are 90.13 mg/g TOC, 72.25 mg/g TOC and 92.01 mg/g TOC for the 20 °C/h heating rate, respectively, whereas the corresponding amounts for the 2 °C/h heating rate in unit of mg/g TOC are 138.17, 108.77 and 120.56 (Fig. 7b, d, f). The generation of methane for all the three types of source rock (Type II_2 and III kerogen) remains increasing distinctly even at the final pyrolysis temperature of 600 °C. This is in contrast with the typical Type I and II kerogens, which usually display a gentle increase trend towards the final pyrolysis temperature of 600 °C (Tian et al., 2007; Wang et al., 2014; Gai et al., 2018).

With the pyrolytic temperature increasing, the dryness index of gaseous hydrocarbon products, represented by the $C_1/(C_1$–$C_5)$ value, is generally declined first and then increased rapidly to 1.0 for all the three samples (Fig. 8a). At the start of heating, yields of both liquid and gaseous hydrocarbons are minor. Liquid hydrocarbons would begin to be generated rapidly with heating, leading to a decrease of the dryness index. Under the 2 °C/h heating rate condition, the minimum values of the dryness index for the mudstone and carbonaceous mudstone are 0.53 and 0.71, respectively, corresponding to a temperature of 360 °C; while that for the coal sample is 0.49 with a corresponding temperature of

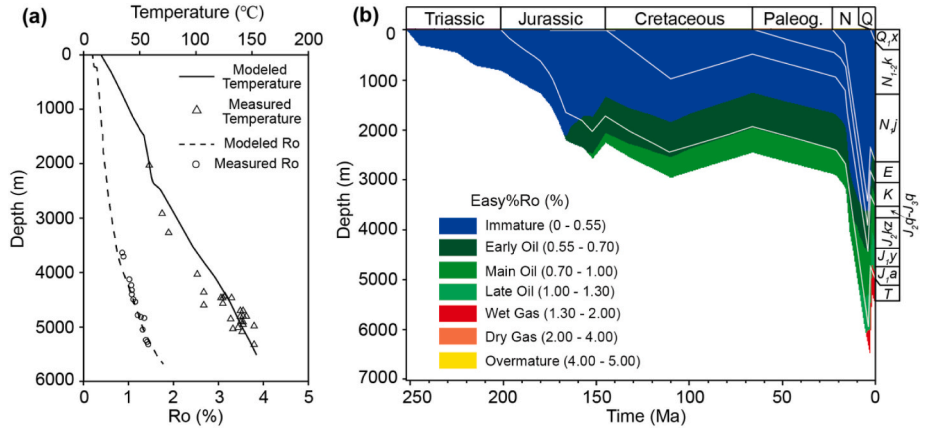

Fig. 13. Modeled burial and maturity evolution of the YN-2 well (see Fig. 1c for location). Left graph showing that the modeled temperature and %Ro curves match the measured data quite nicely.

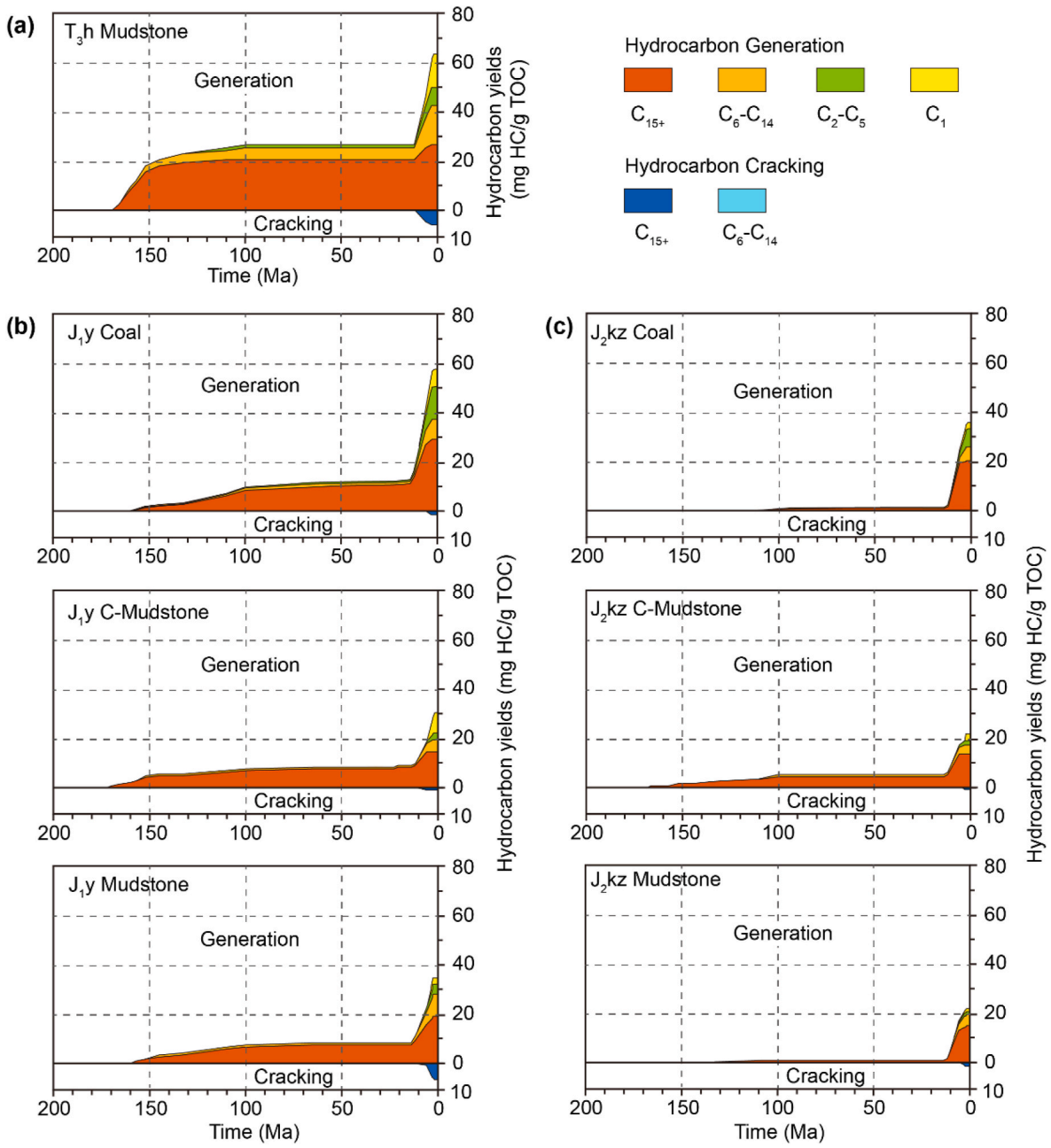

Fig. 14. Hydrocarbon generation and cracking of the source rocks in the YN-2 well. (a) The T_3h mudstone; (b) and (c) are the coal, carbonaceous mudstone and mudstone in the J_1y and J_2kz formations, respectively.

384 °C. The dryness index of gases derived from the carbonaceous mudstone sample is the largest at each heating step, followed by the mudstone and coal samples. This difference could be ascribed to the relative large amount of liquid hydrocarbon generation from the coal sample and the mudstone sample compared with the carbonaceous mudstone sample. For all the source rock samples, the dryness index is close to 1.0 after the pyrolysis temperature reaching 504 °C (2.99 Easy % Ro), indicating that only methane is left above 504 °C.

4.2.3. Inorganic gases

Inorganic gases including CO_2, H_2 and H_2S are detected from the pyrolytic gaseous products with a predominant CO_2 proportion. As carbonate minerals had already been removed during the kerogen extraction procedure, all the measured CO_2 gases would be produced along with the organic thermal degradation, and generated from decarboxylation of organic acids and esters (Huss and Burnham, 1982). The yields of CO_2 increase with temperature for all three samples. The maximum yields of CO_2 for the mudstone, carbonaceous mudstone and coal samples are 310.34 mg/g TOC, 204.78 mg/g TOC and 165.45 mg/g TOC, respectively, at the 2 °C/h heating rate (Fig. 8b), much greater than the amount of organic gases (Fig. 7).

4.3. Hydrocarbon generation and cracking kinetics

On the basis of sealed gold tube pyrolysis experiments, the generation and cracking kinetics of multi-component hydrocarbons are calculated for the first time on the mudstone, carbonaceous mudstone, and coal source rocks in the eastern Kuqa foreland basin.

4.3.1. Kinetics of hydrocarbons generation

Hydrocarbon generation can be described by a set of parallel first-order reactions with a single frequency factor and a discrete activation

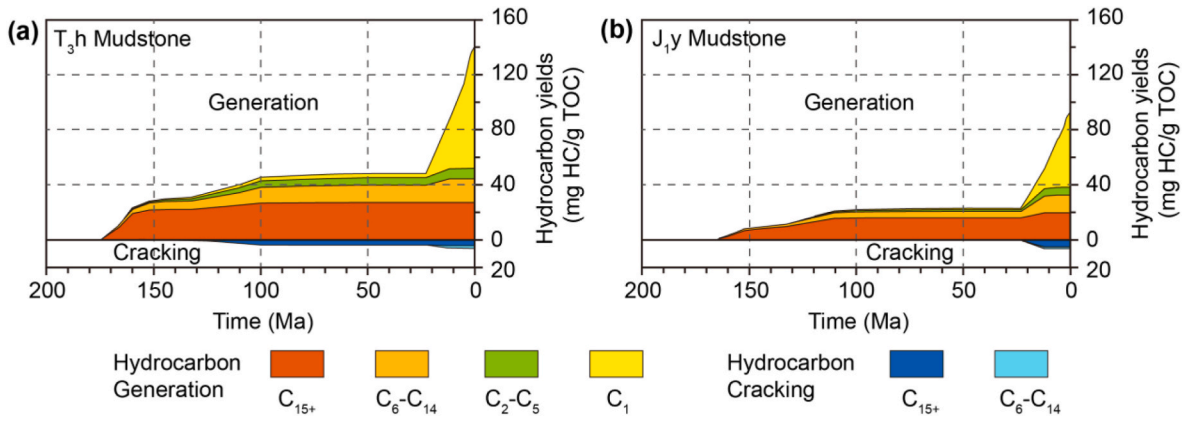

Fig. 15. Hydrocarbon generation and cracking of the T_3h (a) and J_1y (b) source rocks for a pseudo well (PW-1) near the depocenter of the Kuqa foreland basin.

energy (Tang et al., 1996; Behar et al., 1997). Data pairs of pyrolysis temperatures and hydrocarbon yields for the two heating rates before their peak hydrocarbon generation are used to calculate the generative kinetics of different hydrocarbon compositions, including heavier (C_{15+}) and light-to-medium (C_6–C_{14}) liquid hydrocarbons and wet (C_2–C_5) and methane gases. The generative activation energy of C_{15+}, C_6–C_{14}, C_2–C_5 and methane components for the mudstone is in the range of 42–48, 44–54, 49–59, and 54–69 kcal/mol, respectively (Fig. 9a), displaying an overall increasing trend of the dominant activation energy from heavier liquid to gaseous hydrocarbons. The generative activation energies of the four hydrocarbon components for the carbonaceous mudstone and coal samples (40–70 kcal/mol) are similar to that for the mudstone sample (Fig. 9b and c), indicating an easy-to-hard order of hydrocarbon generation. Comparatively, the coal sample has relatively low and narrow ranges of activation energy, especially for the C_{15+}, C_6–C_{14}, and C_2–C_5 components, indicating a much easier hydrocarbon generative capability.

4.3.2. Kinetics of hydrocarbons cracking

After peak hydrocarbon generation, all pyrolytic yields of C_{15+}, C_6–C_{14}, and C_2–C_5 components decrease with further temperature increase, indicating the start of the thermal cracking process of these hydrocarbon components. The cracking amount of each hydrocarbon component at each temperature is calculated from the difference between the maximum generation amount and its measured value for all three samples. The cracking kinetics of the C_{15+}, C_6–C_{14}, and C_2–C_5 components are determined using the data pairs of pyrolysis temperature and its corresponding hydrocarbon cracking amount. The activation energies for the cracking of the C_{15+}, C_6–C_{14}, and C_2–C_5 components are in the range of 48–59 kcal/mol, 58–69 kcal/mol, and 63–74 kcal/mol, respectively, for the mudstone sample, and in the range of 48–61 kcal/mol, 54–63 kcal/mol, and 63–71 kcal/mol, respectively, for the carbonaceous mudstone sample, and in the rage of 51–55, 64–77, and 68–73 kcal/mol, respectively, for the coal sample (Fig. 10).

5. Discussion

5.1. Differential hydrocarbon generation

By integrating the pyrolysis temperatures and their corresponding heating rates, multi-component hydrocarbon yields can be expressed by a more general evaluation factor of thermal maturity, the Easy %Ro of Sweeney and Burnham (1990) (Table 2; Fig. 11). The maximum hydrocarbon yields from the Type I and II_1 kerogens are typically in the range of 300–800 mg/g TOC with a generation peak at around 1.6 (Easy %Ro) (Spigolon et al., 2015; Peng and Jia, 2021; Li et al., 2022). Comparatively, the three source rocks from the eastern Kuqa foreland basin have yielded far less hydrocarbons (<150 mg/g TOC) and reached their generation peaks at final heating temperature equivalent to 4.45% Easy %Ro (Fig. 11). Among the three types of source rock, the mudstone source rock generated the largest amount of gas, followed by the coal and carbonaceous mudstone source rocks. The source rocks in the study area are of gas-prone types, but can generate small amount of oil primarily in mature oil stage (0.7–1.3 %Ro). Relative large amounts of gases can be generated during the over-mature stage (Ro > 2.0%), and gas may still be generated even with maturity greater than 3.0%, showing a significant gas generation capacity among the three source rocks with high to over maturity, consistent with previous studies on the pyrolysis of coaly Type III kerogen (Dieckmann et al., 2006; Erdmann and Horsfield, 2006; Li et al., 2013; Xu et al., 2017).

Different from typical Type I and II_1 kerogens (Peng and Jia, 2021), the three source rocks in the Kuqa foreland basin have a relatively narrower oil generation window. For the mudstone source rock, the C_{15+} and C_6–C_{14} oil components are generated prior to the 0.86% and 1.36% Easy %Ro, respectively, and would begin to be cracked after reaching critical Ro value (Fig. 11a). For the carbonaceous mudstone and the coal source rocks, minor amount of bulk oil can be continuously generated prior to the 1.08% Ro, which would then be gradually cracked to light oil and gases with increasing maturity (Fig. 11b and c). A relatively larger gas-oil ratio was determined during the oil generation stage compared with the Type I and II_1 kerogens, indicating that gases are much easier to be generated in these coaly types of source rocks. Although a certain amount of oil can be generated in the coal source rock, most oil would be absorbed by kerogens in a natural system (Pepper, 1992; Sandvik et al., 1992) and are hard to be expelled, thus providing essential material base for further oil cracking in the source rocks.

The origin of gas generation can be determined using the pyrolysis results of C_1, C_2 and C_3 gases. Previous studies have confirmed that the plot of Ln (C_1/C_2) versus Ln (C_2/C_3) can be utilized to distinguish whether hydrocarbon gases are generated directly from kerogen degradation or from secondary oil cracking (Behar et al., 1991; Prinzhofer and Huc, 1995; Wang et al., 2013). Because similar proportions of ethane and propane are usually yielded during the primary kerogen degradation, the Ln (C_2/C_3) values are almost constant. During the secondary oil cracking stage, more ethane would be generated compared with propane (Wang et al., 2013), causing the Ln (C_2/C_3) values to increase with thermal cracking. The C_1/C_2 ratio is also sensitive to thermal maturity because methane production generally increases more rapidly than that of ethane at a high maturity (Wang et al., 2013). For the 20 °C/h heating rate, all the three source rocks in the Kuqa foreland basin exhibit a decrease in Ln (C_1/C_2) values with a near constant Ln (C_2/C_3) value at the initial heating stage (Ro < 0.96%), indicating gas generation directly from kerogen degradation. A general upward-increasing trend of both Ln (C_1/C_2) and Ln (C_2/C_3) is seen during the stage with Ro greater than 1.19%, showing the contribution

of secondary oil cracking (Fig. 12). There is a slight difference in the beginning of oil cracking among the three types of source rocks, indicating that oil cracking occurs earlier for the mudstone source rock (~Ro > 0.96%) than that for the carbonaceous mudstone and the coal source rocks (~ Ro > 1.19%).

In summary, the three types of coaly bearing source rocks in the Kuqa foreland basin have limited capacity and narrower window for oil generation, and as well as relatively lower hydrocarbon generation capacity and an earlier secondary oil cracking to gas when compared with typical Type I and II_1 kerogens. Therefore, we inferred that multi-layers of source rocks with great thickness (Tang et al., 2021) and massive hydrocarbon generation during high to over mature stages (Liu et al., 2018; Yang et al., 2021) may be the two controlling factors for the formation of this gas-rich basin where several large to giant gas fields have been found. In addition, as large amount of CO_2 would be generated from the three types of source rocks, more attentions need to be paid for it in this field area in further research, because CO_2 gases and related minerals (e.g., calcite, dolomite) are widespread in the lower Jurassic, as well as the Cretaceous and the Paleogene reservoirs (Shi et al., 2018; Zhang et al., 2018; Lai et al., 2019), and thus the densification process of these sandstone reservoirs may be closely related to the charge process of source rock generated CO_2.

5.2. Hydrocarbon generations in the Kuqa foreland basin

The evolution of hydrocarbon generation and cracking of the source rocks in the Kuqa foreland basin has been determined using our specific kinetics on two wells: the Yinan-2 (YN-2) well, a gas producing well on the northern slope, and a pseudo well (PW-1) in the present subsidence center of the basin. Based on the method and input parameters described in Section 3.6, 1D basin models were constructed for both wells. After several iterations, a reasonable burial and thermal model was established for the YN-2 well on the basis of good matches between modeled and measured temperatures and Ro values (Fig. 13). The calibrated heat flow values for the YN-2 well is then applied to model the PW-1 well.

The burial and maturity evolution of the YN-2 well are shown in Fig. 13b. From the Triassic to the Paleogene, source rocks in the upper Triassic and lower to middle Jurassic formations underwent a prolonged period of shallow to moderate burial stage, with the maximum burial depth had never exceeded 3000 m, and entered into early oil to peak oil generation stages (Ro < 1.0%). In the Neogene, huge thicknesses (>3000 m) of sediments were rapidly deposited with the source rocks in the YN-2 well reaching a maximum depth of more than 6000 m. Affected by the late Himalayan orogeny, erosion occurred during the late Neogene to the early Quaternary, followed by a deposition of ~200 m of sediments in the late Quaternary. The Triassic source rock has presently reached a wet gas generation window (1.3 < Ro < 2.0%).

Based on newly acquired specific kinetics for the mudstone, carbonaceous mudstone and coal source rocks in the Kuqa foreland basin, the generation and cracking of the T_3h, J_1y, and J_2kz source rocks in the YN-2 well were reconstructed (Fig. 14).

(1) Two episodes of hydrocarbon generation and expulsion occurred. During the middle Jurassic to early Cretaceous (170–100 Ma), minor amount of liquid hydrocarbons was generated primarily from the T_3h and the J_1y source rocks, while the J_2kz formation generated little hydrocarbons due to its immature nature at that time. From the late Cretaceous to the early Neogene (100–12 Ma), little or no hydrocarbons were generated because the maturity of source rocks remained largely unchanged. During the Neogene Kangcun–Kuqa period (12–3 Ma), large amounts of hydrocarbons were rapidly generated from all the three layers of source rocks. The amount of hydrocarbon generation during this secondary episode is far more than the amount in the earlier hydrocarbon generation stage, representing the crucial moment for hydrocarbon accumulations in the Kuqa foreland basin.

(2) The T_3h mudstone source rock yielded the maximum hydrocarbons per unit because of its deeply burial nature, followed by the J_1y and the J_2kz source rocks. Compared with the mudstone and the carbonaceous mudstone source rocks, the coal source rock generated the maximum amount of hydrocarbon intensity in both J_1y and J_2kz formations.

(3) Hydrocarbon gases from kerogen thermal degradation were mainly generated in the latter (second episode) hydrocarbon generation stage, during which heavier liquid hydrocarbons (C_{15+}) were partially cracked. After the Neogene, both organic matters and liquid hydrocarbons in the source rocks can yield gas.

(4) Although some hydrocarbon gases were generated in the YN-2 area after the Neogene, the percentage to the total gases generated is generally 10%–50%, inconsistent with the actual scale and dryness of the nearby commercial Dibei wet-gas discovery in the area. Therefore, gases from the southern subsidence center with higher maturity are inferred to have contributed the most to the Dibei gas field.

The burial and thermal history of the PW-1 well in the Kuqa foreland basin was used to analyze its hydrocarbon generation and cracking. The pseudo well is located near the present subsidence center and with a maximum depth of ~7000 m. The T_3h mudstone and the J_1y mudstone source rocks (Fig. 15) there also experienced two episodes of hydrocarbon generation, with a similar evolution history as the YN-2 well in the northern slope. Much more dry gases were generated since the Neogene, occupying nearly 67% and 50% of the total generated hydrocarbons in the T_3h and J_1y source rocks, respectively. The start of cracking of heavier liquid hydrocarbons in the PW-1 well occurred at about 120 Ma for the T_3h source rock and around 20 Ma for the J_1y source rock, both of which are earlier than that in the YN-2 well. Massive gases were supplied from the subsidence center of the basin after Neogene, which is essential for the formation of the large gas fields in the area.

In summary, this study (1) has confirmed that the present subsidence center in the Kuqa foreland basin is more significant than the paleo depositional center (Fig. 3), providing an important clue for further hydrocarbon migration studies; (2) has provided a more robust constraint on the oil and gas accumulation processes which have been under ongoing debate (Wang and Long, 2010; Jiang et al., 2015; Guo et al., 2016; Li et al., 2019); and (3) may offer important insight for exploring hydrocarbon exploration targets in the basin in the future (e.g., lithological traps in the slope to sag center in the Kuqa foreland basin).

6. Conclusions

Source rocks in the Kuqa foreland basin, northwestern China are dominated by Type II_2 and III kerogens, with hydrocarbon generation amounts generally less than 150 mg/g TOC. Different from typical Type I and II_1 kerogens, the mudstone, carbonaceous mudstone, and coal source rocks in the Kuqa foreland basin investigated have a generally narrower oil generation window and a comparatively larger gas-oil ratio during the early pyrolysis stage. Gases are much easier to be generated in the coaly type source rock and during the over-mature stage. Significant amount of gases can still be generated at present.

Two episodes of hydrocarbon generations occurred in the Kuqa foreland basin. Hydrocarbon gases were mainly generated during the late evolution stage. At present the depocenter of the Kuqa foreland basin can still supply massive high-maturity gases, providing abundant source for the development of giant gas fields in the basin.

Declaration of competing interest

The authors declare that they have no known competing financial interests or personal relationships that could have appeared to influence

the work reported in this paper.

Data availability

Data will be made available on request.

Acknowledgements

This research was financially supported by the National Natural Science Foundation of China, Grant No. 92055204, 42002115, and 41821002, and the Major Science and Technology Project of PetroChina, Grant No. ZD2019-183-01-04. The authors are grateful to Prof. Hong Lu of the Guangzhou Institute of Geochemistry, Chinese Academy of Sciences for his help with the pyrolysis experiments.

References

Ahmed, K.S., Liu, K., Moussa, H., Liu, J., Ahmed, H.A., Kra, K.L., 2022. Assessment of petroleum system elements and migration pattern of Borno (Chad) Basin, northeastern Nigeria. J. Petrol. Sci. Eng. 208, 109505.
Barth, T., Smith, B.J., Nielsen, S.B., 1996. Do kinetic parameters from open pyrolysis describe petroleum generation by simulated maturation? Bull. Can. Petrol. Geol. 44, 446–457.
Behar, F., Kressman, S., Rudkiewicz, J.L., Vandenbroucke, M., 1992. Experimental simulation in a confined system and kinetic modeling of kerogen and oil cracking. Org. Geochem. 19, 173–189.
Behar, F., Kressmann, S., Rudkiewicz, J.L., Vandenbroucke, M., 1991. Experimental simulation in a confined system and kinetic modelling of kerogen and oil cracking. Adv. Org. Geochem. 19, 173–189.
Behar, F., Vandenbroucke, M., Tang, Y., Marquis, F., Espitalie, J., 1997. Thermal cracking of kerogen in open and closed systems: determination of kinetic parameters and stoichiometric coefficients for oil and gas generation. Org. Geochem. 26, 321–339.
Bohacs, K.M., Carroll, A.R., Neal, J.E., Mankiewicz, P.J., 2000. Lake-basin type, source potential, and hydrocarbon character: an integrated-sequence-stratigraphic–geochemical framework. In: Gierlowski-Kordesch, E.H., Kelts, K.R. (Eds.), Lake Basins through Space and Time, AAPG Studies in Geology, vol. 46, pp. 3–34.
Braun, R.L., Burnham, A.K., 1994. KINETICS: a computer program to analyze chemical reaction data. Lawrence Livermore National Laboratory Report, UCRL-ID-21588. Rev. 2 (September 1994), 14.
Braun, R.L., Burnham, A.K., 1987. Analysis of chemical reaction kinetics using a distribution of activation energies and simpler models. Energy Fuel. 1, 153–161.
Burnham, A.K., Braun, R.L., 1999. Global kinetic analysis of complex materials. Energy Fuel. 13, 1–22.
Burnham, A.K., Braun, R.L., 1990. Development of a detailed model of petroleum formation, destruction, and expulsion from lacustrine and marine source rocks. Org. Geochem. 16, 27–39.
Chen, J.P., Zhao, C.Y., He, Z.H., 1997. Criteria for evaluating the hydrocarbon generating potential of organic matter in coal measures. Petrol. Explor. Dev. 24 (1), 1–5 (in Chinese with English abstract).
Dieckmann, V., 2005. Petroleum formation from heterogeneous source rocks, new insight from kinetic modelling and geological predictions. Mar. Petrol. Geol. 22, 375–390.
Dieckmann, V., Ondrak, R., Cramer, B., Horsfield, B., 2006. Deep basin gas: new insights from kinetic modeling and isotopic fractionation in deep-formed gas precursors. Mar. Petrol. Geol. 23, 183–199.
Du, J., Wang, Z., Hu, S., Wang, Q., Xie, H., 2012. Formation conditions and geological characteristics of deep giant gas provinces in the Kuqa foreland thrust belt. Petrol. Explor. Dev. 39 (4), 413–422.
Erdmann, M., Horsfield, B., 2006. Enhanced late gas generation potential of petroleum source rocks via recombination reactions: evidence from the Norwegian North Sea. Geochem. Cosmochim. Acta 70, 3943–3956.
Espitalié, J., Madec, M., Tissot, J., Menning, J., Leplat, P., 1977. Source rock characterization method for petroleum exploration. Proc. Ninth Annual Offshore Technol. Conf. 3, 439–448.
Gai, H., Tian, H., Xiao, X., 2018. Late gas generation potential for different types of shale source rocks: implications from pyrolysis experiments. Int. J. Coal Geol. 193, 16–29.
Gao, G., Liang, H., Li, H., Jiao, L., Wang, Z., Hou, Q., 2009. Organic geochemistry of carboniferous and lower permian source rocks, turpan-hami basin, NW China. Petrol. Explor. Dev. 36 (5), 583–592 (in Chinese with English abstract).
Graham, S.A., Hendrix, M.S., Wang, L.B., 1993. Collision successor basin of western China: impact of tectonic inheritance on sand composition. Geol. Soc. Am. Bull. 105, 323–344.
Guo, X., Liu, K., Jia, C., Song, Y., Zhao, M., Zhuo, Q., Lu, X., 2016. Hydrocarbon accumulation processes in the Dabei tight-gas reservoirs, Kuqa subbasin, Tarim Basin, northwest China. AAPG Bull. 100 (10), 1501–1521.
Hantschel, T., Kauerauf, A.I., 2009. Fundamentals of Basin and Petroleum Systems Modeling. Springer Dordrecht Heidelberg London, New York, p. 476pp.
Hao, F., Zou, H., Gong, Z., Deng, Y., 2007. Petroleum migration and accumulation in the Bozhong sub-basin, Bohai Bay basin, China: significance of preferential petroleum migration pathways (PPMP) for the formation of large oilfields in lacustrine fault basins. Mar. Petrol. Geol. 24, 1–13.
Harouna, M., Pigott, J., Philp, R., 2017. Burial history and thermal maturity evolution of the termit basin, Niger. J. Petrol. Geol. 40 (3), 277–297.
He, D.F., Li, D.S., He, J.Y., Wu, X.Z., 2013. Comparison in petroleum geology between Kuqa depression and southwest depression in Tarim Basin and its exploration significance. Acta Pet. Sin. 34, 201–218 (in Chinese with English abstract).
Hendrix, M.S., Graham, S.A., Carroll, A.R., Sobel, E.R., McKnight, C.L., Schuleim, B.J., Wang, Z., 1992. Sedimentary record and climatic implications of recurrent deformation in the tian Shan: evidence from mesozoic strata of the north Tarim, south junggar, and turpan basins, northwest China. Geol. Soc. Am. Bull. 104, 53–79.
Horsfield, B., Disko, U., Leistner, F., 1989. The micro-scale simulation of maturation: outline of a new technique and its potential applications. Geol. Rundsch. 78, 361–373.
Hu, S., Wang, X., Cao, Z., Li, J., Gong, D., Xu, Y., 2020. Formation conditions and exploration direction of large and medium gas reservoirs in the Junggar Basin, NW China. Petrol. Explor. Dev. 47 (2), 266–279.
Huang, W.K., Zeng, L.F., Pan, C.C., Xiao, Z.Y., Zhang, H.Z., Huang, Z.B., Zhao, Q., Yu, S., Xu, H., Chen, C.S., Liu, D.Y., Liu, J.Z., 2019. Petroleum generation potentials and kinetics of coaly source rocks in the Kuqa Depression of Tarim Basin, northwest China. Org. Geochem. 133, 32–52.
Huss, E.B., Burnham, A.K., 1982. Gas evolution during pyrolysis of various Colorado oil shales. Fuel 61, 1188–1196.
Jasper, K., Krooss, B.M., Flajs, G., Hartkopf-Fröder, Chr, Littke, R., 2009. Characteristics of type III kerogen in coal-bearing strata from the Pennsylvanian (Upper Carboniferous) in the Ruha Basin, Western Germany: comparison of coals, dispersed organic matter, kerogen concentrates and coal-mineral mixtures. Int. J. Coal Geol. 80, 1–19.
Jia, C.Z., 1992. Evolution of the Tarim plate. In: Li, Q.B., Dai, J.X., Liu, R.Q., Li, J.L. (Eds.), Glossary of the Contemporary Geological Researches (I). Nanjing University Publishing House, pp. 22–31 (in Chinese).
Jia, C.Z., Gu, J.Y., Zhang, G.Y., 2002. Geological constraints of giant and medium-sized gas fields in Kuqa Depression. Chin. Sci. Bull. 47, 47–54.
Jia, C.Z., He, D.F., Lu, H.M., 2004. Episodes and geodynamic setting of Himalayan movement in China. Oil Gas Geol. 25, 121–125 (in Chinese with English abstract).
Jiang, Z.X., Li, F., Yang, H.J., Li, Z., Liu, L.F., Chen, L., Du, Z.M., 2015. Development characteristics of factures in Jurassic tight reservoir in Dibei area of Kuqa depression and its reservoir-controlling model. Acta Pet. Sin. 36, 102–111.
Jin, Z.J., 2005. New advancement in research of China's typical superimposed basins and reservoirs (part I): classification and research methods of superimposed basins. Oil Gas Geol. 26, 553–562 (in Chinese with English abstract).
Jin, Z.J., Yang, M.H., Lv, X.X., Sun, D.S., Tang, X., Peng, G.X., Lei, G.L., 2008. The tectonics and petroleum system of the Qiulitagh fold and thrust belt, northern Tarim basin, NW China. Mar. Petrol. Geol. 25, 767–777.
Katz, B.J., 1995. Lacustrine source rock systems—is the Green River Formation an appropriate analog? Geol. Geofiz. 36, 26–41.
Lai, J., Fan, X.C., Pang, X.J., Zhang, X.S., Xiao, C.W., Zhao, X.J., Han, C., Wang, G.W., Qin, Z.Q., 2019. Correlating diagenetic facies with well logs (conventional and image) in sandstones: the Eocene–Oligocene Suweiyi Formation in Dina 2 Gasfield, Kuqa depression of China. J. Petrol. Sci. Eng. 174, 617–636.
Lewan, M.D., Ruble, T.E., 2002. Comparison of petroleum generation kinetics by isothermal hydrous and non-isothermal open-system pyrolysis. Org. Geochem. 33, 1457–1475.
Li, E., Pan, C., Yu, S., Jin, X., Liu, J., 2013. Hydrocarbon generation from coal, extracted coal and bitumen rich coal in confined pyrolysis experiments. Org. Geochem. 64, 58–75.
Li, E., Pan, C., Yu, S., Jin, X., Liu, J., 2016. Interaction of coal and oil in confined pyrolysis experiments: insight from the yields and carbon isotopes of gas and liquid hydrocarbons. Mar. Petrol. Geol. 69, 13–37.
Li, J., Wang, C., Li, J., Ma, W., Zhang, H.Z., Lu, Y.H., Li, D.J., Liu, M.C., 2019. Source and exploration direction of tight oil and gas in the Dibei section of northern Kuqa depression. Chin. Petrol. Explor. 24 (4), 485–497 (in Chinese with English abstract).
Li, K., Zhao, Z.F., Lu, H., Liu, X.R., Peng, P.A., Hsu, C.S., 2022. Effects of inherent pyrite on hydrocarbon generation by thermal pyrolysis: an example of low maturity type-II kerogen from Alum shale formation, Sweden. Fuel 312, 122865.
Li, X.Q., Xiao, X.M., Mi, J.K., Tang, Y.C., Xiao, Z.Y., Liu, D.H., Shen, J.G., Liu, J.Z., 2005. Kinetic parameters of methane generated from source rocks and its application in the Kuqa Depression of the Tarim Basin. Acta Geol. Sin. 79 (1), 133–142 (in Chinese with English abstract).
Li, X.Q., Xiao, X.M., Tang, Y.C., Xiao, Z.Y., Mi, J.K., Liu, D.H., Shen, J.G., Liu, J.Z., 2004. Gas generation and accumulation in the Yinan-2 gas field, Kuqa Depression. Chin. Sci. Bull. 49 (Suppl. p), 100–106 (in Chinese).
Liu, J.L., Liu, K.Y., Jiang, Z.X., Gui, L.L., Li, F.L., 2018. Hydrocarbon accumulation processes in the Yangtake foldbelt, Kuqa foreland basin, NW China: insight from integrated basin modelling and fluid inclusion analyses. J. Petrol. Geol. 41 (4), 447–466.
Liu, J.L., Jiang, Z.X., Liu, K.Y., Gui, L.L., Xing, J.Y., 2016. Hydrocarbon sources and charge history in the southern slope region, Kuqa foreland basin, northwestern China. Mar. Petrol. Geol. 74, 26–46.
Lu, H., Greenwood, P., Chen, T.S., Liu, J.Z., Peng, P.A., 2011. The role of metal sulfates in thermochemical sulfate reduction (TSR) 471 of hydrocarbons: insight from the yields and stable carbon isotopes of gas products. Org. Geochem. 42, 700–706.
Lu, X.S., Liu, K.Y., Zhuo, Q.G., Zhao, M.J., Liu, S.B., Fang, S.H., 2012. Palaeo-fluid evidence of the multi-stage hydrocarbon charges in Kela-2 gas field, Kuqa foreland basin. Tarim Basin. Petrol. Explor. Develop. 39, 574–582.

Lu, X., Zhao, M., Liu, K., Zhuo, Q., Fan, J., Yu, Z., Gong, Y., 2018. Formation condition of deep gas reservoirs in tight sandstones in Kuqa Foreland Basin. Petrol. Res. 3, 346–358.
Mangotra, S.R., Chari, M.V.N., Thomas, N.J., Mishra, K.N., Chandra, K., 1995. Determination and analysis of optimal kinetic parameters for hydrocarbon generation from source rock sequences of Cambay basin. India. Org. Geochem. 23 (5), 371–378.
Pan, C., Geng, A., Zhong, N., Liu, J., Yu, L., 2009. Kerogen pyrolysis in the presence and absence of water and minerals: amounts and compositions of bitumen and liquid hydrocarbons. Fuel 88, 909–919.
Peng, P.A., Jia, C.Z., 2021. Evolution of deep source rock and resource potential of primary light oil and condensate. Acta Pet. Sin. 42 (12), 1543–1555 (in Chinese with English abstract).
Pepper, A.S., Corvi, P.J., 1995. Simple kinetic models of petroleum formation: Part I—oil and gas generation from kerogen. Mar. Petrol. Geol. 12, 291–319.
Pepper, A.S., 1992. Estimating of petroleum expulsion behavior of source rocks: a novel quantitative approach. In: England, A.J., Fleet, A.J. (Eds.), Petroleum Migration, vol. 59. Geol. Soc. Spec. Publ., pp. 9–31
Peters, K.E., 1986. Guidelines for evaluating petroleum source rock using programmed pyrolysis. AAPG Bull. 70, 318–329.
Peters, K.E., Burnham, A.K., Walters, C.C., 2015. Petroleum generation kinetics: single versus multiple heating-ramp open-system pyrolysis. AAPG Bull. 99 (4), 591–616.
Peters, K.E., Walters, C.C., Mankiewicz, P.J., 2006. Evaluation of kinetic uncertainty in numerical models of petroleum generation. AAPG Bull. 90 (3), 387–403.
Prinzhofer, A.A., Huc, A.Y., 1995. Genetic and post-genetic molecular and isotopic fractionations in natural gases. Chem. Geol. 126, 281–290.
Quigley, T.M., MacKenzie, A.S., Gray, J.R., 1987. Kinetic theory of petroleum generation. In: Doligez, B. (Ed.), Migration of Hydrocarbons in Sedimentary Basins. Editions Technip, Paris, pp. 649–665.
Ritter, U., Myhr, M.B., Vinge, T., Aareskjold, K., 1995. Experimental heating and kinetic models of source rocks: comparison of different methods. Org. Geochem. 23, 1–9.
Sandvik, E.I., Young, W.A., Curry, D.J., 1992. Expulsion from hydrocarbon sources: the role of organic absorption. Org. Geochem. 19, 77–87.
Schenk, H.J., Horsfield, B., 1993. Kinetics of petroleum generation by programmed temperature closed- versus open-system pyrolysis. Geochem. Cosmochim. Acta 57, 623–630.
Schenk, H.J., Horsfield, B., Krooss, B., Schaefer, R.G., Schwochau, K., 1997. Kinetics of petroleum formation and cracking. In: Welte, D.H., Horsfield, B., Backer, D.R. (Eds.), Petroleum and Basin Evolution. Springer, Berlin, pp. 233–269.
Shi, H., Luo, X.R., Yang, H.J., Lei, G.L., Tang, Y.G., Zhang, L.K., Lei, Y.H., 2018. Sources of quartz grains influencing quartz cementation and reservoir quality in ultra-deeply buried sandstones in Keshen-2 gas field, north-west China. Mar. Petrol. Geol. 98, 185–198.
Spigolon, A.L.D., Lewan, M.D., Penteado, H.L.B., Coutinho, L.F.C., Filho, J.G.M., 2015. Evaluation of the petroleum composition and quality with increasing thermal maturity as simulated by hydrous pyrolysis: a case study using a Brazilian source rock with Type I kerogen. Org. Geochem. 83–84, 27–53.
Sweeney, J.J., Burnham, A.K., 1990. Evaluation of a simple model of Vitrinite reflectance based on chemical kinetics. AAPG Bull. 74 (10), 1559–1570.
Tang, Y., Jenden, P.D., Nigrini, A., Teerman, S.C., 1996. Modeling early methane generation in coal. Energy Fuel. 10, 659–671.
Tang, Y.G., Yang, X.Z., Xie, H.W., Xu, Z.P., Wei, H.X., Xie, Y.N., 2021. Tight gas reservoir characteristics and exploration potential of jurassic Ahe Formation in Kuqa depression, Tarim Basin. Chin. Petrol. Explor. 26 (4), 113–124 (in Chinese with English abstract).
Taylor, G.H., Teichmüller, M., Davis, A., Diessel, C.F.K., Littke, R., Robert, P., 1998. Organic Petrology. Schweizerbart), Stuttgart, p. 704.
Tegelaar, E.W., Noble, R.A., 1994. Kinetics of hydrocarbon generation as a function of the molecular structure of kerogen as revealed by pyrolysis-gas chromatography. Org. Geochem. 22, 543–574.
Tian, H., Xiao, X.M., Wilkins, R.W.T., Li, X.Q., Gan, H.J., 2007. Gas sources of the YN2 gas pool in the Tarim Basin- Evidence from gas generation and methane carbon isotope fractionation kinetics of source rocks and crude oils. Mar. Petrol. Geol. 24, 29–41.
Tian, J., Wang, Q.H., Yang, H.J., Li, Y., 2021. Petroleum exploration history and enlightenment in Tarim Basin. Xinjing Pet. Geol. 42 (3), 272–282 (in Chinese with English abstract).
Tian, J., Yang, H.J., Wu, C., Mo, T., Zhu, W.H., Shi, L.L., 2020. Discovery of Well Bozi-9 and ultra-deep natural gas exploration potential in the Kelasu tectonic zone of the Tarim Basin. Nat. Gas. Ind. 40 (1), 11–19 (in Chinese with English abstract).
Tian, Z.J., Luo, Z.L., Luo, Z.T., 1996. Awati intracontinental foreland basin in Xinjiang. Oil Gas Geol. 17, 282–306 (in Chinese with English Abstract).
Tissot, B.P., Pelet, R., Ungerer, P., 1987. Thermal history of sedimentary basins, maturation indices, and kinetics of oil and gas generation. AAPG Bull. 71, 1445–1466.
Ungerer, P., 1990. State of the art of research in kinetic modeling of oil formation and expulsion. Org. Geochem. 16, 1–25.
Ungerer, P., Pelet, R., 1987. Extrapolation of the kinetics of oil and gas formation from laboratory experiments to sedimentary basins. Nature 327, 52–54.
Vyazovkin, S., Burnham, A.K., Criado, J.M., Pérez-Maqueda, L.A., Popescu, C., Sbirrazzuoli, N., 2011. ICTAC Kinetics Committee recommendations for performing kinetic computations on thermal analysis data. Thermochim. Acta 520, 1–19.
Vyazovkin, S., Wight, C.A., 1999. Model-free and model-fitting approaches to kinetic analysis of isothermal and non-isothermal data. Thermochim. Acta 340–341, 53–68.
Wang, L.S., Li, C., Liu, S.W., Li, H., Xu, M.J., Wang, Q., Ge, R., Jia, C.Z., Wei, G.Q., 2003. Geotemperature gradient distribution of Kuqa foreland basin, north of Tarim, China. Chin. J. Geophys. 46, 403–407 (in Chinese with English abstract).
Wang, Z., Long, H., 2010. Different hydrocarbon accumulation histories in the kelasu-yiqikelike structural belt of the Kuqa foreland basin. Acta Geol. Sin. 84, 1195–1208.
Wang, Q., Lu, H., Shen, C., Liu, J., Peng, P., Hsu, C.S., 2014. The impact of inorganically bound sulfur on late shale gas generation. Energy Fuel. 28, 785–793.
Wang, Q.T., Liu, W.H., Meng, P.L., Hu, J.L., Wang, X.F., Zhang, D.D., Liu, J.Z., 2021. Assessment the gas potential of coal-bearing mudstones from upper paleozoic in ordos basin via gold-tube pyrolysis. J. Nat. Gas Sci. Eng. 90, 103895.
Wang, Q.T., Lu, H., Greenwood, P., Shen, C.C., Liu, J.Z., Peng, P.A., 2013. Gas evolution during kerogen pyrolysis of Estonian Kukersite shale in confined gold tube system. Org. Geochem. 65, 74–82.
Wang, Y., Li, P., Feng, Z., Shao, H., Jia, Z., Xia, Y., Wang, Z., 2023. Geochemical characteristics of shales from the first member of Qingshankou Formation in Gulong Sag, Songliao Basin, China: implication for mechanism of organic matter enrichment. Mar. Petrol. Geol. 150, 106142.
Waples, D.W., Suizu, M., Kamata, H., 1992. The art of maturity modeling: Part 2—Alternative models and sensitivity analysis. AAPG Bull. 76, 47–66.
Wygrala, B.P., 1989. Integrated study of an oil field in the southern Po basin, northern Italy. Ph.D thesis. Berichte des Forschungszentrums Juelich 217.
Xu, H., Ding, X., Luo, Z., Liu, C., Li, E., Huang, P., Yu, S., Liu, J., Zou, Y., Pan, C., 2017. Confined pyrolysis for simulating hydrocarbon generation from Jurassic coaly source rocks in the Junggar Basin, Northwest China. Energy Fuel. 31, 73–94.
Xu, J., Liu, Z., Bechtel, A., Sachsenhofer, R.F., Jia, J., Meng, Q., Sun, P., 2019b. Organic matter accumulation in the upper cretaceous qingshankou and nenjiang formations, Songliao basin (NE China): implications from high-resolution geochemical analysis. Mar. Petrol. Geol. 102, 187–201.
Xu, S., Hao, F., Xu, C., Zou, H., Zhang, X., Zong, Y., Zhang, Y., Cong, F., 2019a. Hydrocarbon migration and accumulation in the northwestern bozhong subbasin, Bohai Bay basin, China. J. Petrol. Sci. Eng. 172, 477–488.
Xu, X., Xu, S., Liu, J., Chen, L., Liang, H., Mei, L., Liu, Z., Shi, W., 2021. Thermal maturation, hydrocarbon generation and expulsion modeling of the source rocks in the baiyun sag, pearl river mouth basin, south China sea. J. Petrol. Sci. Eng. 205, 108781.
Yang, X.W., Tian, J., Wang, Q.H., Li, Y.L., Yang, H.J., Li, Y., Tang, Y.G., Yuan, W.F., Huang, S.Y., 2021. Geological understanding and favorable exploration fields of ultra-deep formations in Tarim Basin. Chin. Petrol. Explor. 26 (4), 17–28 (in Chinese with English abstract).
Yang, X.W., Wang, Q.H., Li, Y., Lv, X.X., Xie, H.W., Wu, C., Wang, C.L., Wang, X., Mo, T., Wang, R., 2022. Formation mechanism of the Bozi-Dabei trillion cubic natural gas field, Kuqa foreland thrust belt. Earth Sci. Front. 29 (6), 175–187 (in Chinese with English abstract).
Zhang, E., Hill, R.J., Katz, B.J., Tang, Y., 2008. Modeling of gas generation from the Cameo coal zone in the Piceance Basin, Colorado. AAPG Bull. 92 (8), 1077–1106.
Zhang, L.Q., Yan, Y.M., Luo, X.R., Wang, Z.B., Zhang, H.Z., 2018. Diagenetic differences of tight sandstone of the lower jurassic Ahe Formation in the yiqikelike area of the Kuqa depression, Tarim Basin. Earth Sci. Front. 25 (2), 170–178.
Zhang, S.C., Zhang, B., Zhu, G.Y., Wang, H.T., Li, Z.X., 2011. Geochemical evidence for coal-derived hydrocarbons and their charge history in the Dabei gas field, Kuqa thrust belt, Tarim Basin, NW China. Mar. Petrol. Geol. 28, 1364–1375.
Zhao, M.J., Zhang, B.M., 2002. Source rocks for a giant gas-accumulation area in the Kuqa Foreland Depression. Chin. J. Geol. 37 (Suppl. p), 35–44 (in Chinese with English abstract).
Zhao, W., Zou, C., Wang, Z., Li, J., Li, M., Niu, J., 2004. The intension and signification of "Sag-wide Oil-Bearing Theory" in the hydrocarbon-rich depression with terrestrial origin. Petrol. Explor. Dev. 31 (2), 5–13 (in Chinese with English abstract).
Zou, Y.R., Zhao, C.Y., Wang, Y.P., Zhao, W.Z., Peng, P.A., Shuai, Y.H., 2006. Characteristics and origin of natural gases in the Kuqa depression of Tarim Basin, NW China. Org. Geochem. 37, 280–290.